Drivers of late Miocene tropical sea surface cooling: a new perspective from the equatorial Indian Ocean

Claire Martinot[1], Clara T. Bolton[1], Anta-Clarisse Sarr[1], Yannick Donnadieu[1], Marta Garcia[1], Emmeline Gray[1,2], Kazuyo Tachikawa[1]

[1]Aix Marseille Univ, CNRS, IRD, INRAE, Coll France, CEREGE, Aix-en-Provence, France

[2]Now at: School of Environment, Earth and Ecosystem Sciences, The Open University, Milton Keynes, UK

Corresponding authors: Claire Martinot (martinot@cerege.fr) or Clara Bolton (bolton@cerege.fr)

Key Points:

- New late Miocene orbital-resolution Mg/Ca sea surface temperature record from the eastern equatorial Indian Ocean spanning 9 to 5 Ma
- Tropical cooling is >3°C; new model simulations suggest that a pCO2 decrease from 560 to 300 ppm could account for most of this cooling
- Increase in meridional sea surface temperature gradients over the late Miocene more modest than previously suggested

Abstract

During the late Miocene, global cooling occurred alongside the establishment of near-modern terrestrial and marine ecosystems. Significant (3 to 5 °C) sea surface cooling from 7.5 to 5.5 Ma is recorded by proxies at mid to high latitudes, yet the magnitude of tropical cooling and the role of atmospheric carbon dioxide (pCO_2) in driving this trend are debated. Here, we present a new orbital-resolution sea surface temperature (SST) record spanning the late Miocene to earliest Pliocene (9 to 5 Ma) from the eastern equatorial Indian Ocean (International Ocean Discovery Program Site U1443) based on Mg/Ca ratios measured in tests of the planktic foraminifer *Trilobatus trilobus*. Our SST record reveals a 3.2 °C decrease from 7.4 to 5.8 Ma, significantly increasing previous estimates of late Miocene tropical cooling. Analysis of orbital-scale variability shows that before the onset of cooling, SST variations were dominated by precession-band (19-23 kyr) variability, whereas tropical temperature became highly sensitive to obliquity (41 kyr) after 7.5 Ma, suggesting an increase in high latitude forcing. We compare a revised global SST database with new paleoclimate model simulations and show that a pCO_2 decrease from 560 ppm to 300 ppm, in the range suggested by pCO_2 proxy records, could explain most of the late Miocene sea surface cooling observed at Site U1443. Estimation of meridional sea surface temperature gradients using our new Site U1443 record as representative of tropical SST evolution reveals a much more modest increase over the late Miocene than previously suggested, in agreement with modelled gradients.

Plain Language Summary

The late Miocene is an interesting time period for paleoclimatologists because the Earth underwent important climatic and ecological changes that led to the establishment of our modern climate. An important cooling of global surface oceans was recorded by tracers used to reconstruct past temperature, however the amplitude of this cooling in the tropics and the role of atmospheric carbon dioxide (CO_2) in driving it are unclear. We present a new reconstruction of surface temperatures from the eastern equatorial Indian Ocean based on the temperature-dependent ratio of magnesium to calcium measured in fossil shells of zooplankton (Foraminifera). Our results reveal a cooling (3.2 °C) higher than previous estimates of tropical ocean cooling (1 to 2.5 °C). To understand the role of atmospheric CO_2 in driving this cooling

we simulated Miocene climate using a complex model, and find that an atmospheric CO_2 decrease from 560 ppm to 300 ppm could explain most of the reconstructed surface ocean cooling. We also find that ocean surface temperature gradient between the tropics (using our new reconstruction) and the northern high latitudes shows a more modest increase over the late Miocene than suggested by previous studies, in agreement with new and existing climate model results.

1 Introduction

The late Miocene (11.6 to 5.3 million years ago, Ma) offers the opportunity to assess the sensitivity of Earth's climate system to changing internal (ice volume and vegetation induced albedo changes, greenhouse gas concentrations) and external (orbital forcing) drivers in a warmer than modern world, yet with a continental configuration similar to modern (Knorr et al., 2011; Herbert et al., 2016; Holbourn et al., 2018; Steinthorsdottir et al., 2021). The late Miocene lies in a context of long-term global cooling and declining partial pressures of atmospheric CO_2 (pCO_2) that started at the end of the Early Eocene Climate Optimum (~49 Ma) (e.g. Beerling & Royer, 2011; Westerhold et al., 2020; Rae et al., 2021). Subsequent cooling and decreasing pCO_2 led to the progressive establishment of polar ice sheets, with two major phases of Antarctic ice sheet expansion preceding the late Miocene: the first initiating at the Eocene/Oligocene Transition ~34 Ma and the second at 13.9 Ma during the Middle Miocene Climatic Transition (e.g. Flower & Kenett, 1994; Zachos et al, 1996, 2001; Lear et al., 2000; Westerhold et al., 2020). The establishment of a permanent and large-scale Northern Hemisphere ice sheet occurred in the late Pliocene to earliest Pleistocene, with an intensification of Northern Hemisphere glaciation at ~2.7 Ma (e.g. Balco & Rovey 2010; Bailey et al., 2012; Shakun et al., 2016).

During the late Miocene, major global sea surface cooling is recorded in both hemispheres despite the absence of a strong trend in deep-ocean foraminiferal $\delta^{18}O$ that might imply sustained global cooling (Herbert et al., 2016; Westerhold et al., 2020). This occurs alongside major ecological events recorded both on land and in the marine environment. The establishment of near modern ecosystems, with the expansion of deserts in north Africa and central Asia (Pound et al., 2012; Zhang et al., 2014) and the rise to dominance of C4 grassland biomes in tropical and

subtropical regions between 10 and 3.5 Ma, may have been driven by aridification and/or a decrease in pCO_2, although the diachronous nature of the C4 ecosystem expansion implies additional regional drivers (e.g. fire severity, seasonality, and rainfall amount) (Cerling et al., 1997; Pagani et al., 1999; Herbert et al., 2016; Andrae et al., 2018; Carrapa et al., 2019; Tauxe & Feakins, 2020). In the oceans, late Miocene changes in calcifying phytoplankton geochemistry and morphology are interpreted to show adaptation to decreasing CO_2 availability (Bolton & Stoll, 2013; Bolton et al 2016). The late Miocene carbon isotope shift (LMCIS, defined by a ~1 ‰ decrease in benthic foraminiferal $\delta^{13}C$ from 7.9 to 6.4 Ma), recorded worldwide in benthic and planktic foraminiferal $\delta^{13}C$, provides further evidence for a major change in global carbon cycling at this time (Keigwin, 1979; Keigwin & Shackleton, 1980; Holbourn et al., 2018; Bolton et al. 2021; Drury et al., 2021). Between 7 and 5 Ma, episodic occurrences of ice rafted debris recorded in North Atlantic (Larsen et al, 1994; John & Krissek, 2002) and North Pacific (Krissek, 1995) sediments are associated with short positive excursions in benthic foraminiferal $\delta^{18}O$, suggesting the development of small ephemeral ice sheets in South-east Greenland and South-east Alaska at this time (Hodell et al., 2001; Holbourn et al., 2018; Jöhnck et al., 2020). The hypothesis that small, dynamic Northern Hemisphere ice sheets were present in the late Miocene is supported by the observation that obliquity influence on global climate cycles (benthic $\delta^{18}O$ and $CaCO_3$ content) increased after 13 Ma and became dominant after ~7.7 Ma, suggesting an amplification of high-latitude forcing (Drury et al., 2017; Drury et al 2021; Holbourn et al., 2018; Westerhold et al., 2020). Taken together, these studies suggest that profound changes in climate dynamics occurred in the late Miocene, with important cryosphere and carbon cycle changes and a parallel reorganization of terrestrial biomes. Yet, the exact role of pCO_2 in the evolution of late Miocene climate and ecosystem change is unclear because existing pCO_2 reconstructions are generally low-resolution, with divergent trends between proxies. Certain studies (e.g. Kürschner et al 1996; Pagani et al., 1999, 2005; Retallack 2009; Zhang et al., 2013) show no major pCO_2 decrease during the late Miocene, whereas other studies either directly (Bolton et al., 2016; Mejia et al., 2017; Stoll et al 2019; Tanner et al., 2020; Rae et al., 2021) or indirectly (Bolton & Stoll, 2013) support the hypothesis that pCO_2 gradually decreased over this interval.

A recent study of sea surface temperatures (SSTs) reconstructed using the C_{37} alkenone unsaturation index ($U^{k'}_{37}$ index) revealed a global cooling from 7.5 to 5.5 Ma (the Late Miocene Global Cooling, LMCG), with a magnitude comprised between 3 and 5 °C in high and mid-latitudes and a modest cooling of ~1 °C in the tropics (Herbert et al., 2016). While the linear relation between the $U^{k'}_{37}$ index and temperature is well defined for temperatures between 8 and 24 °C, it contains larger uncertainties at warmer temperatures (> 24 °C) due to a decrease in $U^{k'}_{37}$ sensitivity to temperature (e.g. Sonzogni et al 1997; Conte et al., 1998; Grimalt et al., 2001; Pelejero & Calvo, 2003; Conte et al., 2006; Tierney & Tingley, 2018). Thus, it is likely that tropical SSTs prior to the LMGC and the long-term amplitude of cooling recorded by the $U^{k'}_{37}$ index are underestimated (Herbert et al., 2016). Several low-resolution tropical Pacific temperature records based on the TEX_{86} index also span the late Miocene, showing 2 to 4 °C of cooling (Zhang et al., 2014; Liu et al., EGU abstract 2020). SST estimates based on planktic foraminiferal Mg/Ca ratios from the South China Sea (Steinke et al., 2010; Holbourn et al., 2018) also suggest 2.5 °C of late Miocene cooling. However, existing late Miocene tropical SST records are either from upwelling areas (Arabian Sea and Equatorial Pacific; Huang et al., 2007; Rousselle et al, 2013; Zhang et al., 2014; Herbert et al., 2016), or from regions affected by complex local oceanography (South China Sea and Andaman Sea; Holbourn et al., 2018; Jöhnck et al., 2020), precluding the resolution of long-term, global tropical SST trends. Therefore, there is a clear need to reconstruct tropical SSTs in open-ocean, warm-pool regions, characterized by the warmest SSTs in the world oceans (>28 °C) (e.g. Lukas & Webster 1989; Vinayachandran & Shetye, 1991; Yan et al., 1992; Wang & Enfield, 2001), using optimal proxies.

Here, we present new orbital-resolution SST estimates from sediments deposited at International Ocean Discovery Program (IODP) Site U1443, in the eastern equatorial Indian Ocean, spanning the late Miocene (9 to 5 Ma). SSTs are estimated using Mg/Ca ratios measured on the mixed layer dwelling foraminifer *Trilobatus trilobus*. Accurate age control is provided by a new orbitally tuned benthic foraminiferal $\delta^{18}O$ record generated on specimens picked from the same samples (Bolton et al., 2021). To test the idea that a pCO_2 decrease drove global sea surface cooling during the late Miocene, as suggested by recent studies (e.g. Herbert et al., 2016; Tanner et al., 2020; Rae et al., 2021), we present new climate model simulations using the Earth System Model IPSL-CM5A2 (Sepulchre et al., 2020). We evaluate the effect of pCO_2 on tropical SSTs

and latitudinal SST gradients using three different pCO_2 scenarios within the range suggested by late Miocene pCO_2 proxy data (300, 420 and 560 ppm), and compare modelled SSTs to our new Site U1443 SST record as well as a revised global SST data compilation.

2 Site Description and modern oceanography

IODP Site U1443 is located in the southernmost Bay of Bengal (BOB) and was cored during Expedition 353 on the crest of the Ninetyeast Ridge (5° 23' 2.94'' N, 90° 21' 40.381'' E, 2924 meters water depth) (Clemens et al., 2016). Site U1443 is a re-drill of ODP Site 758 (Shipboard Scientific Party, 1989). Due to the northward displacement of the Indian Plate, Site U1443 was located at a paleolatitude of 2.7°N at 9 Ma and 4°N at 5 Ma (Scotese, 2016).

In the modern northern Indian Ocean, seasonal South Asian monsoon circulation patterns are the dominant control on oceanographic conditions (Webster et al., 1998). Seasonal variations of insolation and pressure gradients between the southern subtropical Indian Ocean and the Asian continent induce a large-scale shift in surface wind direction and speed with strong southwesterlies during the summer monsoon (June, July, August) and weaker northeasterlies during the winter monsoon (December, January, February) over the BOB (Tomczak & Godfrey, 2001). The BOB is also marked by a complete seasonal reversal of surface ocean circulation (Schott et al., 2009), with saltier, denser water masses from the Arabian Sea entering the BOB via the Southwest Monsoon Current during summer and less saline water masses from the BOB flowing into the Arabian Sea via the Northeast Monsoon Current during winter (Jensen, 2001 and 2003) (Figure 1a-b). In addition, the BOB receives a large amount of freshwater from direct rainfall and riverine inputs. This large input of freshwater and its redistribution by horizontal advection lead to the formation of strong salinity stratification governed by the seasonal and spatial variability of the barrier layer thickness (Shetye et al., 1996; Thadathil et al., 2007). The formation of a barrier layer between the base of the mixed layer and the top of the thermocline inhibits interactions between shallow and intermediate water masses, allowing BOB surface waters to maintain warm temperatures (>28 °C) throughout the year (Rao & Sivakumar, 2003; Thadathil et al., 2007). As a consequence, seasonal SST variability in the BOB is mainly

controlled by the strength of (monsoonal) wind-driven mixing (e.g. Unger et al., 2003; Vidya et al., 2013) and by salinity stratification (barrier layer formation). In waters overlying Site U1443, strong southwesterlies result in maximum annual surface ocean wind stress, deeper wind-driven mixing and reduced stratification during the summer monsoon (Figure 1c). The intrusion of high salinity Arabian Sea water during summer also acts to deepen the mixed layer (Thadathil et al., 2007), resulting in average SSTs of 28.7 °C (Figure 1c), very close to mean annual SST (28.8 °C). In autumn and early winter, the progressive southward spreading of fresh water from riverine inputs in the northern BOB results in the development of salinity stratification and a barrier layer (Thadathil et al., 2007) and allows relatively warm SSTs (> 28.1 °C; Figure 1c) to persist above Site U1443. During this time the lowest sea surface salinities occur (33.6 to 33.8 PSU; Zweng et al., 2018), although the annual sea surface salinity range is small (33.6 to 34.35 PSU; Figure 1c) compared to further north in the BOB. SSTs reach a maximum of 29.9 °C in April, when lowest surface ocean wind stress results in strong stratification and a shoaling of the mixed layer (Figure 1c). In summary, local ocean-atmosphere processes induce a relatively small annual SST variability in waters overlying Site U1443 (28.1-29.9 °C; Figure 1c; Locarnini et al., 2018), thus we consider this site suitable for reconstructing “open ocean” tropical SSTs that are representative of the global picture.

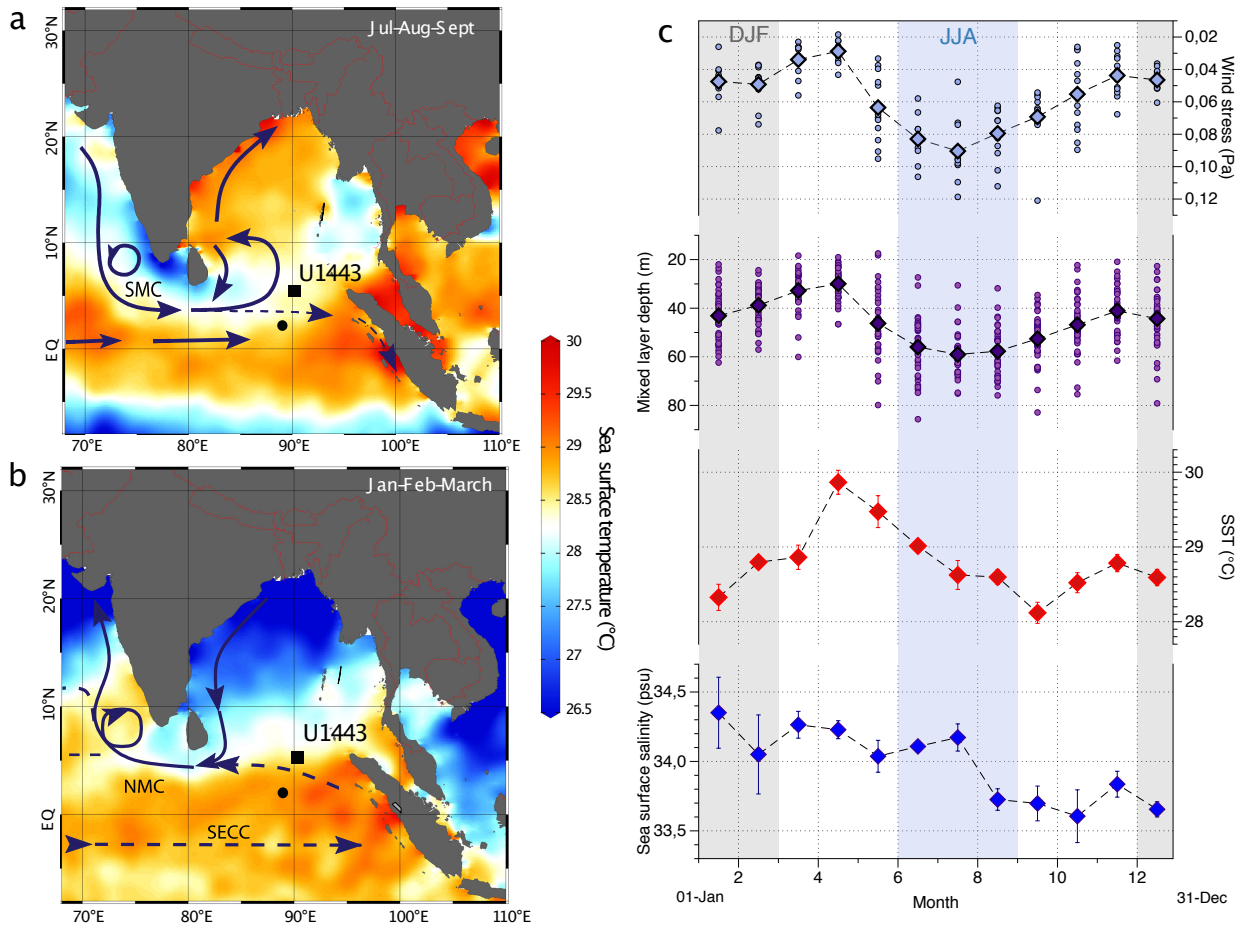

Figure 1. Modern oceanographic conditions at Site U1443 in the southern Bay of Bengal. Maps show seasonal SST and surface ocean circulation (arrows) during the summer (July, August, September) (a) and during the winter (January, February, March) (b). On both maps the modern location of IODP Site U1443 in the Bay of Bengal (black square) and its paleolocation at 9 Ma (latitude ~2.5°N and longitude ~89°E; black dot) are shown. Panel (c) shows modern monthly wind stress and mixed layer depth, with points representing individual months and diamonds with line representing monthly mean values over entire time series, and sea surface temperature and sea surface salinity with diamonds with lines corresponding to statistical mean of monthly mean values over entire time series with standard error bars, above Site U1443. Maps were created with Ocean Data View software using the SST datasets from the World Ocean Atlas 2013 (Locarnini et al., 2013). Paleolocation of Site U1443 was calculated from GPlates software using rotations and plate boundaries from the PALEOMAP PaleoAtlas for Gplates (Scotese, 2016). Ocean circulation is from Schott et al. (2009). SMC: Southwest Monsoon Current, NMC: Northeast Monsoon Current, SECC: South Equatorial Counter Current. In panel

(c) wind stress is from ERDDAP (Wind Stress, Metop-A ASCAT, 0.25°, Global, Near Real Time, 2009-present), mixed layer depth (1969-2010) is from Keerthi et al. (2013), SST and SSS are from the World Ocean Atlas 2018 (Locarnini et al., 2018 and Zweng et al., 2018). Datasets were extracted for a box between 4.5-5.5°N latitude and 89-91°E longitude (depending on grid resolution) and binned by month. JJA: June, July, August, DJF: December, January, February.

3 Materials and Methods

3.1 Sampling and *Trilobatus trilobus* taxonomy and ecology

Site U1443 samples used in this study are from the revised shipboard splice comprised between 122.6 m and 70.06 m CCSF-A (Core Composite depth below Sea Floor), from Core U1443B-7H-5W to Core U1443C-15H-4W, spanning the late Miocene-earliest Pliocene (9 to 5 Ma) (Bolton et al., 2021). Sediments are dominated by calcareous nannofossil ooze with well-preserved shell of foraminifera (~70-80 % $CaCO_3$ with slightly increasing clay content upcore) (Clemens et al., 2016). Bulk samples were washed through a 63 μm sieve with tap water, then the coarse fraction was oven dried at 50 °C. We apply the age model of Bolton et al. (2021), based on revised biostratigraphy and tuning of benthic foraminiferal $\delta^{18}O$ to an eccentricity-tilt target, which results in sedimentation rates between 0.5 and 1.9 cm/kyr. We selected 735 samples over the 9 to 5 Ma interval for Mg/Ca SST reconstruction, with a mean resolution of 5.5 kyr.

In each sample 50 to 60 tests of *Trilobatus trilobus* (Reuss, 1850) were picked from the 212-315 μm size fraction, avoiding individuals with gametogenic calcite that could introduce a cold bias due to migration during gametogenesis (Bé, 1980; Hemleben et al., 2012). In the modern ocean, *T. trilobus* is considered to be one of four morphospecies of the *Trilobatus sacculifer* plexus (Spezzaferri et al., 2015; Poole & Wade 2019). It ranges stratigraphically from the lower Miocene to recent (Spezzaferri 1994) and is very abundant in the tropical to subtropical oceans (Bé & Tolderlund, 1971; Schiebel & Hemleben, 2017). *T. trilobus* is a spinose, photosymbiont-bearing species that is therefore constrained to the upper photic zone, calcifying in the mixed layer, with low seasonality in stratified tropical waters (Schiebel & Hemleben, 2017). *T. trilobus*

tests were abundant and well preserved throughout the late Miocene at Site U1443 (see section 4.1).

3.2 Mg/Ca-SST reconstruction

3.2.1 Mg/Ca Cleaning and Analysis

Trilobatus trilobus tests were weighed, gently crushed between two glass slides to open chambers, then fragments were homogenized before cleaning. Test fragments were cleaned to remove clay and organic matter, following the short "Mg cleaning" protocol of Barker et al. (2003) without a reductive step. A cleaning test was performed on ten samples throughout the study interval to test the sensitivity of measured Mg/Ca ratios to the inclusion of a reductive cleaning step (Rosenthal et al., 2004) (Text S1 and Figure S1). Samples were dissolved in 0.075 M HNO_3 and centrifuged to remove potentially remaining detrital particles (Greaves et al., 2005), then the solution was diluted with 2 % HNO_3. Samples were analyzed using bracketing to minimize instrumental drift with an ICP-QMS (Agilent 7500ce) at CEREGE. Together with Mg/Ca and Sr/Ca ratios, Fe, Al and Mn concentrations were analyzed. Long term precision determined by analysis of independent in-house standards during each run over 2 years is on average 0.56 % (r.s.d) for Mg/Ca. In nine samples, *T. trilobus* tests were also picked from the 355-500 μm size fraction and analyzed following identical protocols described above to access the sensitivity of Mg/Ca to test size (Text S2 and Figure S2).

3.2.2 Calibration

We compare SSTs reconstructed using three different *T. sacculifer* exponential calibration equations: the commonly-applied Anand et al. (2003) sediment trap calibration from the Sargasso Sea ("Mg cleaning", test size: 350-500 μm), the Dekens et al. (2002) calibration based on core top data from the tropical Pacific Ocean, which includes a basin-specific dissolution correction ("Cd cleaning", test size: 250-350 μm), and the Hollstein et al. (2017) calibration based on Western Pacific Warm Pool core-top data ("Cd-cleaning", test size: 250-355 μm) (Figure S3). Because we find no systematic bias of Mg/Ca ratio according to cleaning method

and test size (Texts S1-2 and Figures S1-2), we select the Dekens et al. (2002) calibration (Equation 1).

$$Mg/Ca = 0.37.\exp^{0.09[T-0.36(\text{core depth km})-2.0°C]} \quad (1)$$

Core-top *T. trilobus* Mg/Ca ratios at Site U1443 (Mg/Ca = 3.74 ± 0.19 to 3.79 ± 0.19 mmol/mol, measured in four Holocene samples from the upper 8 cm of the core; G. Marino, unpublished data) yield reconstructed SSTs of 28.2 to 29.4 °C with this calibration, consistent with the modern mean annual SST range above the site (28.1 to 29.9 °C). In contrast, the Anand et al. (2003) calibration produces much cooler temperatures of 25.8 to 26.5 °C and the Hollstein et al. (2017) calibration produces slightly cooler temperatures of 27.8 to 29 °C when applied to Site U1443 core-top Mg/Ca values. The choice of calibration does not affect reconstructed SST trends (Figure S3).

3.2.3 Correction for Mg/Ca_{sw}

The residence time of Ca (~1.1 million years) and Mg (~13 million years) in the ocean (Broecker & Peng, 1982) suggest that Mg/Ca of seawater (Mg/Ca_{sw}) in the late Miocene may have been significantly different to the present-day value of 5.2 mmol/mol (Evans & Muller 2012). Thus, for reconstructions older than 1.1 Ma, it is necessary to correct Mg/Ca measured in foraminiferal tests for the effect of secular variations in Mg/Ca_{sw} (e.g. Evans & Muller, 2012; Tierney et al. 2019). Cenozoic reconstructions of Mg/Ca_{sw} are based on a variety of proxies including fluid inclusions in halite (Horita et al., 2001; Lowenstein et al., 2001), calcium carbonate veins (Coggon et al., 2010), benthic foraminifera (Lear et al., 2000), echinoderms (Dickson et al., 2002) and corals (Gothmann et al., 2015). However, the history of Mg/Ca_{sw} is still poorly constrained by proxies, in particular for the late Miocene where data are sparse, and various modelling scenarios have also been proposed (Figure S4). We compared modelling scenarios and selected the HS15 scenario (Higgins & Schrag, 2015) based on pore fluid chemistry modelling for Mg/Ca_{sw} correction in this study (see Text S3 for rationale). The effect of Mg/Ca_{sw} variations on Mg/Ca_{test} was corrected following the approach of Tierney et al. (2019) with a linear

relationship with H=1 instead of a power law relationship (Evans & Muller, 2012). Both of these Mg/Ca_{sw}-Mg/Ca_{test} relationships are based on the same data derived from the *T. sacculifer* culture experiment in Delaney et al., (1985), thus we prefer to use the linear relation as it provides a simpler approach.

$$Mg/Ca_{test}^{t=t} = \frac{Mg/Ca_{sw}^{t=t\ H}}{Mg/Ca_{sw}^{t=0\ H}} \times B.exp^{AT} \qquad (2)$$

In Text S4, we discuss the effect of different H values and the impact of Mg/Ca_{sw} correction on reconstructed SSTs.

3.3 Error propagation and time series analyses

Propagated Mg/Ca-SST ±1σ and 2σ uncertainties linked to analytical and age model errors were estimated via a bootstrap Monte Carlo procedure using the Paleo-Seawater Uncertainty Solver (PSU Solver; Thirumalai et al., 2016) in Matlab. The age model uncertainty used is 20 kyr and the average analytical uncertainty for Mg/Ca data is 0.02 mmol/mol. Uncertainties related to Mg/Ca_{sw} are not included in the error propagation, and different scenarios are shown in Figure S5. 10 000 Monte Carlo iterations were performed.

Time series analyses were performed using the software package Acycle (Li et al., 2019) and cross-wavelet analyses were performed in R using the biwavelet package (Grinsted et al., 2004; Gouhier et al., 2016), on records resampled at constant 2 kyr intervals to preserve maximum resolution, and filtered to remove periodicities longer than one third of dataset length (>1.3 Ma). Evolutive and singular spectral analyses were performed with the Fast Fourier transform (LAH) method (Kodama & Hinnov, 2014) and the Multi Taper Method (Thomson, 1982), respectively. For evolutive analyses of Mg/Ca from Site U1443 a window of 800 kyr and a step of 100 kyr were used. Where records overlap (~8 to 5 Ma), our Site U1443 Mg/Ca record was compared to the South China Sea ODP Site 1146 Mg/Ca record (Holbourn et al., 2018), and LAH was performed with a window of 600 kyr and a step of 100 kyr. Cross-wavelet analyses were performed on Mg/Ca and benthic $\delta^{18}O$ records from site U1443, both records were resampled and filtered as described above.

3.4 Late Miocene SST modelling and data compilation

To simulate the effect of late Miocene pCO_2 decrease on tropical Indian Ocean SSTs we used the Earth System Model IPSL-CM5A2 (Sepulchre et al., 2020) that simulates the interactions between ocean, atmosphere, land and ice. The IPSL-CM5A2 coupled model is a combination of the LMDZ5A atmospheric model (Hourdin et al., 2013), the ORCHIDEE land surface model (Krinner et al., 2005) and the NEMOv3.6 oceanic model (Madec, 2015) that includes an ocean dynamic component (OPA; Madec, 2018), a sea-ice thermodynamics model (LIM2; Fichefet & Maqueda, 1997; Timmermann et al., 2005) and a biogeochemistry model (PISCES-v2; Aumont et al., 2015). The ocean component has a horizontal resolution of 2° by 2° (refined to 0.5° in the tropics) and 31 vertical levels, whose thickness increases from 10 m at the surface to 500 m at the bottom. The atmospheric component has a horizontal resolution of 1.875° in latitude by 3.75° in longitude with 39 vertical levels. The ocean-atmosphere coupling is ensured by the OASIS3-MCT 2.0 coupler (Valcke, 2013) that interpolates and exchanges variables between the two components.

We used the late Miocene paleogeography from Sarr et al. (in review) that is based on PLIOMIP (Haywood et al., 2020) with additional manual modifications. Those include a more exposed Sundaland and the Australian continent located further south relative to its modern position, which result in a wider Indonesian Gateway that connects West Pacific and tropical Indian Ocean water masses via Indonesian Throughflow (ITF). Other differences include a closed Bering Strait and the absence of Hudson Bay. A small ice-sheet is present on Greenland and the size of the Antarctic Ice Sheet is reduced compare to present-day, with the removal of the West Antarctic ice sheet. Given the range of pCO_2 reconstructed by various proxies for the late Miocene (1 to 3 times preindustrial values of 280 ppm, see section 5.2), we designed three simulations with atmospheric pCO_2 values of 300, 420 and 560 ppm respectively. The solar constant was set at 1364.3 $W.m^{-2}$ and orbital parameters were kept at modern values.

To enable comparison between existing SST records and our new Indian Ocean record, as well as a model-data comparison, we compiled all available late Miocene Mg/Ca, $U^{k'}_{37}$, and TEX_{86} data and recalculated SSTs using consistent calibrations and corrections. Mg/Ca-SSTs (Holbourn et al., 2018; Jöhnck et al., 2020) were recalculated using the Dekens et al. (2002) calibration and a Mg/Ca_{sw} correction as described in Section 3.2. $U^{K'}_{37}$-SSTs (Huang et al., 2007; Rommerskirchen et al., 2011; LaRiviere et al., 2012; Rousselle et al., 2012; Seki et al., 2012; Zhang et al., 2014; Herbert et al., 2016; Liu et al., 2019) were recalculated using the BAYSPLINE calibration to account for the attenuation of the $U^{k'}_{37}$ responses to SST at temperatures >24 °C (Tierney & Tingley, 2018). TEX_{86}-SSTs (Zhang et al., 2014; Super et al., 2020) were recalculated using the BAYSPAR calibration analog mode (Tierney & Tingley, 2015). We then compared our revised global SST compilation, averaged over two one-million-year time windows centred on 8 and 6 Ma, to modelled latitudinal SST gradients. We chose these time windows to represent SSTs before and after the LMGC while excluding the effect of short term/orbital-scale variability, and to investigate the potential role of pCO_2 in driving this long-term cooling. To calculate the paleopositions at 6 and 8 Ma for each site, we used GPlates software (http://www.gplates.org), using rotations and plate boundaries from the PALEOMAP PaleoAtlas for Gplates (Scotese, 2016).

4 Results

4.1 Validity of Mg/Ca_{foram} for SST reconstruction at Site U1443

Indicators of cleaning performance and test dissolution suggest that our Mg/Ca record is suitable for SST reconstruction (Figure S6). Fe/Ca, Al/Ca and Mn/Ca show no correlation with Mg/Ca (Figure S6a-c), suggesting that the influence of clay minerals and manganese oxides on foraminiferal Mg/Ca is negligible. Test dissolution preferentially removes Mg (Brown & Elderfield, 1996; Lea et al., 1999; Rosenthal et al., 2000; Dekens et al., 2002) and lowers foraminiferal test weight (Rosenthal & Lohman, 2002; Lea et al., 2006) and the percentage of coarse fraction (Bassinot et al., 1994). It is also possible that foraminiferal Sr/Ca decreases as carbonate dissolution advances (Stoll et al., 1999). We find no correlation between Mg/Ca ratio and Sr/Ca, mean mass of individual tests, or % coarse fraction (Figure S6d-f), which gives us

confidence that dissolution is unlikely to have influenced temporal variations in Mg/Ca. Scanning Electron Microscope (SEM) images of *T. trilobus* tests in selected samples also attest to their good preservation (Figure S6). Tests are devoid of secondary inorganic calcite crystals on their surface and inner walls, easily identifiable at the micron scale (Edgar et al., 2015; Sexton et al., 2006), and the pore structure appears well preserved. Cross-section images of test walls show a microgranular texture without secondary calcite crystals, suggesting that the initial biogenic structure of the test is preserved.

In certain regions, strong seasonality in planktic foraminiferal production and shell flux can bias Mg/Ca SST records away from mean annual values (e.g. Jonkers et al., 2010, 2013). In the region of Site U1443, annual SST variability is small (~1.7 °C), and two productivity maxima occur over the annual cycle. The largest primary productivity peak occurs during late summer (July, August, September; mean SST 28.5 °C) and a second peak is observed in winter (December, January, February; mean SST 28.6 °C) (Rixen et al., 2019; Bolton et al., 2021). The seasonality of planktonic foraminiferal mass fluxes recorded at a southern Bay of Bengal sediment trap site seems to broadly follow annual primary productivity and are highest during July, September and January (Ramaswamy & Gaye, 2006). Thus, even if foraminiferal shell fluxes were biased towards high productivity seasons, temperatures recorded by *T. trilobus* at Site U1443 are still representative of mean annual mixed-layer temperatures (28.8 °C), with a possible small bias towards cooler SSTs (less than −0.3 °C).

Some studies have demonstrated that planktic foraminiferal Mg/Ca can be highly sensitive to salinity and pH changes in some species (Mathien-Blard & Bassinot, 2009; Allen et al., 2016; Gray & Evans 2019). Above Site U1443, modern sea surface salinity is close to the open-ocean value of ~34 PSU and seasonal variations are small (< 1 PSU). Tierney et al. (2019) suggest that SST sensitivity to salinity is low between 33 and 38 PSU. Thus, we consider a monsoon-related salinity influence on Mg/Ca at this site to be unlikely. In cultures of *T. sacculifer,* no pH effect on Mg/Ca is detected (Allen et al., 2016; Gray & Evans 2019), thus, calibration equations do not include a term to correct for the pH effect (Gray & Evans, 2019; Tierney et al. 2019). In summary, Mg/Ca ratios measured in *T. trilobus* are interpreted as representative of past mean

annual temperatures in the upper mixed layer of the ocean above Site U1443, with negligible influence of salinity or pH.

4.2 Orbital-scale SST variability

Late Miocene SSTs at Site U1443 show significant (up to 3 °C amplitude) orbital-scale variability, which is unaffected by Mg/Ca_{sw} correction. During certain Thvera-Gilbert (TG) cold stages (Shackleton et al., 1995) recorded in benthic oxygen isotopes from the same site (Bolton et al., 2021), coolings of 0.7 to 2.3 °C are recorded (Figure 2). The Mg/Ca record is characterized by >99 % significant variability at the orbital periods 41 kyr, 24 kyr and 20 kyr, and at the non-primary orbital periods 49 and 59 kyr (Figure 3). At the onset of the LMGC around 7.7 to 7.5 Ma, 41 kyr and 49 kyr cycles emerge (Figure 3c), and before 7.5 Ma precession-band variability (24 and 20 kyr) is more pronounced (Figure 3d). Evolutive spectral analysis of the Mg/Ca record also shows variability at the ~400 kyr (Figure 3b) period, but this period is only >95 % significant in the interval before 7.5 Ma (Figure 3d). Pronounced periods at 225 and 231 kyr (> 99 % significant) are also identified in the Mg/Ca spectrum, and two well-defined ~200 kyr cycles are visible between 9 and 8.6 Ma (Figures 2-5).

4.3 Long term SST trends at Site U1443

Mg/Ca shows a slightly increasing trend from 9 to 7.4 Ma, with values comprised between 3.90 and 2.67 mmol/mol (mean = 3.24 mmol/mol, n = 345, SD = 0.45 °C; Figure 2a). Mg/Ca ratios then decrease between 7.4 and 5.8 Ma by 0.55 mmol/mol, reaching a minimum average value of 2.81 mmol/mol between 6.2 and 5.8 Ma (Figure 2a). Values then increase from 5.8 to 5 Ma by 0.2 mmol/mol. Reconstructed SSTs (uncorrected and corrected for Mg/Ca_{sw} variations) show the same long-term trends and structure as raw Mg/Ca data, with higher SSTs in the oldest part of the record, a long-term gradual cooling from 7.4 to 5.8 Ma, an SST minimum at 5.8 Ma followed by a warming between 5.8 and 5 Ma during the latest Miocene-early Pliocene (Figure 2a). With no Mg/Ca_{sw} correction, calculated SSTs over the whole record vary between 23.7 °C and 29.2 °C with a mean value of 26.7 °C (Figure 2a, blue curve). Application of our preferred correction for secular changes in Mg/Ca_{sw} (see Methods, Texts S3-4) increases absolute SST estimates by 2.5 to 4.9 °C relative to uncorrected SSTs, and increases the slope of reconstructed long-term

cooling by 31 % (Figures 2a and S5). Corrected SSTs vary between 26.7 °C and 34.1 °C with a mean value of 30.4 °C (*n*=735, SD= 1.35°C), and are above the modern and core-top range prior to 6.5 Ma and close to or within the modern range between 6.5 and 5 Ma (Figure 2a, red curve). The warmer temperatures from 9 to 7.4 Ma fluctuate between 29.6 °C and 34.1 °C with a mean of 31.6 °C (*n*=345, SD 0.7 °C). This warm period is followed by a gradual cooling of 3.2 °C from 7.4 to 5.8 Ma. From 5.8 Ma until the Miocene-Pliocene transition at 5.3 Ma, SST increases by 1 °C.

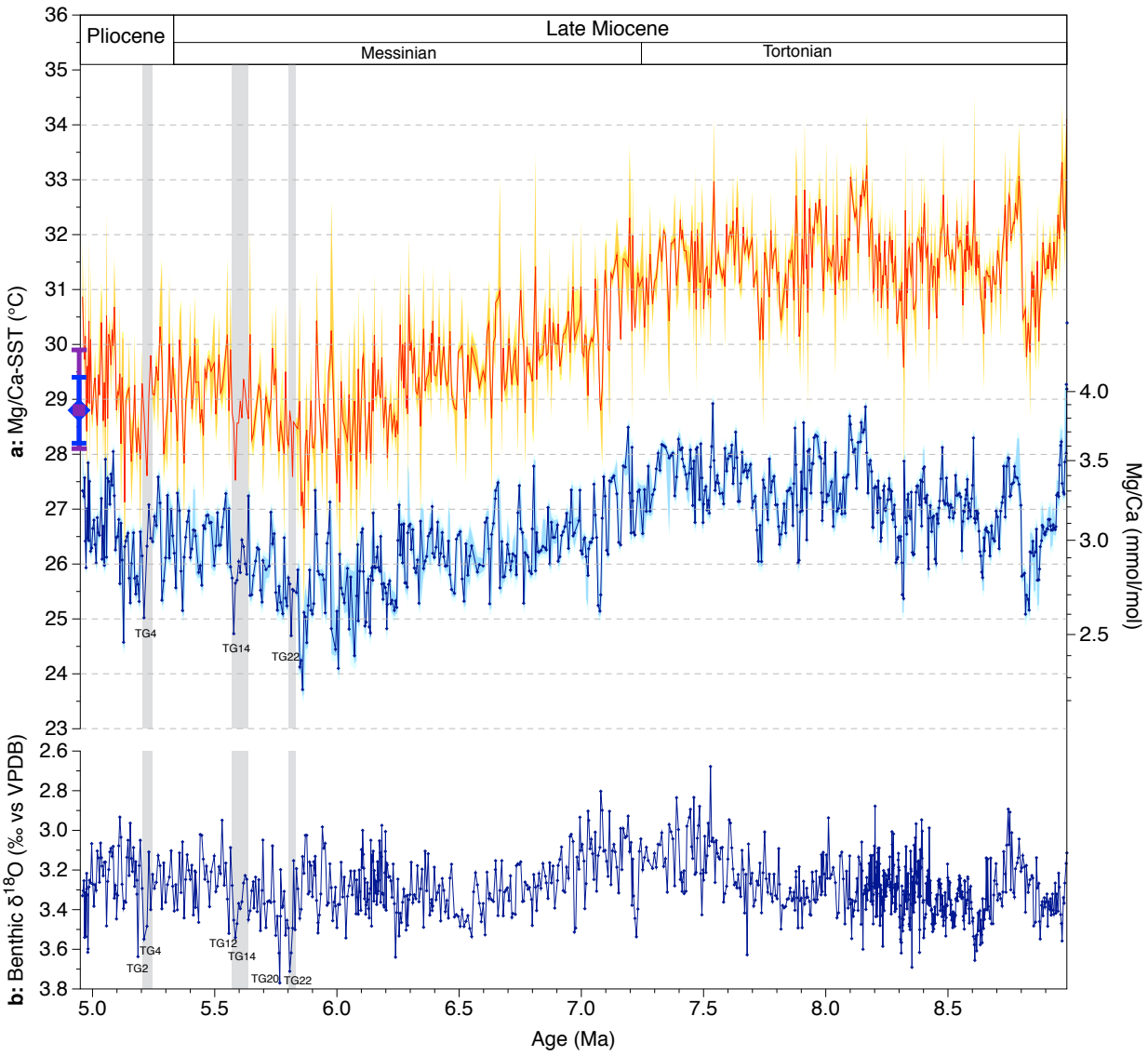

Figure 2. Late Miocene Mg/Ca-SST reconstruction from Site U1443.

(a) SST reconstruction derived from Mg/Ca ratios in *T. trilobus*, calculated using the Dekens et al. (2002) *T. sacculifer* equation for the Pacific. The blue curve shows SST uncorrected for

448 Mg/Ca_{sw} variation, and measured Mg/Ca ratios are also shown on the right axis. The red curve is
449 SST corrected for Mg/Ca_{sw} variation following the scenario of HS15 (see section 3.2) with a
450 linear relation between Mg/Ca_{test} and Mg/Ca_{sw} (H=1). The SST error envelopes correspond to
451 $\pm 1\sigma$ and $\pm 2\sigma$ uncertainty (including analytical and age model errors) estimated using PSU Solver
452 (Thirumalai et al., 2016). On the left axis the blue diamond represents mean core top Mg/Ca-SST
453 with SD (blue error bar) and purple square represents mean annual SST for modern with
454 max/min seasonal SST (purple error bar) (Holocene; 28.8 ±0.6 °C; G. Marino, unpublished and
455 modern SST 28.8 °C +1.1 °C and -0.7 °C; World Ocean Atlas 2018). (b) Site U1443 benthic
456 $\delta^{18}O$ (Bolton et al., 2021) with some Thvera-Gilbert (TG) cold stages indicated.

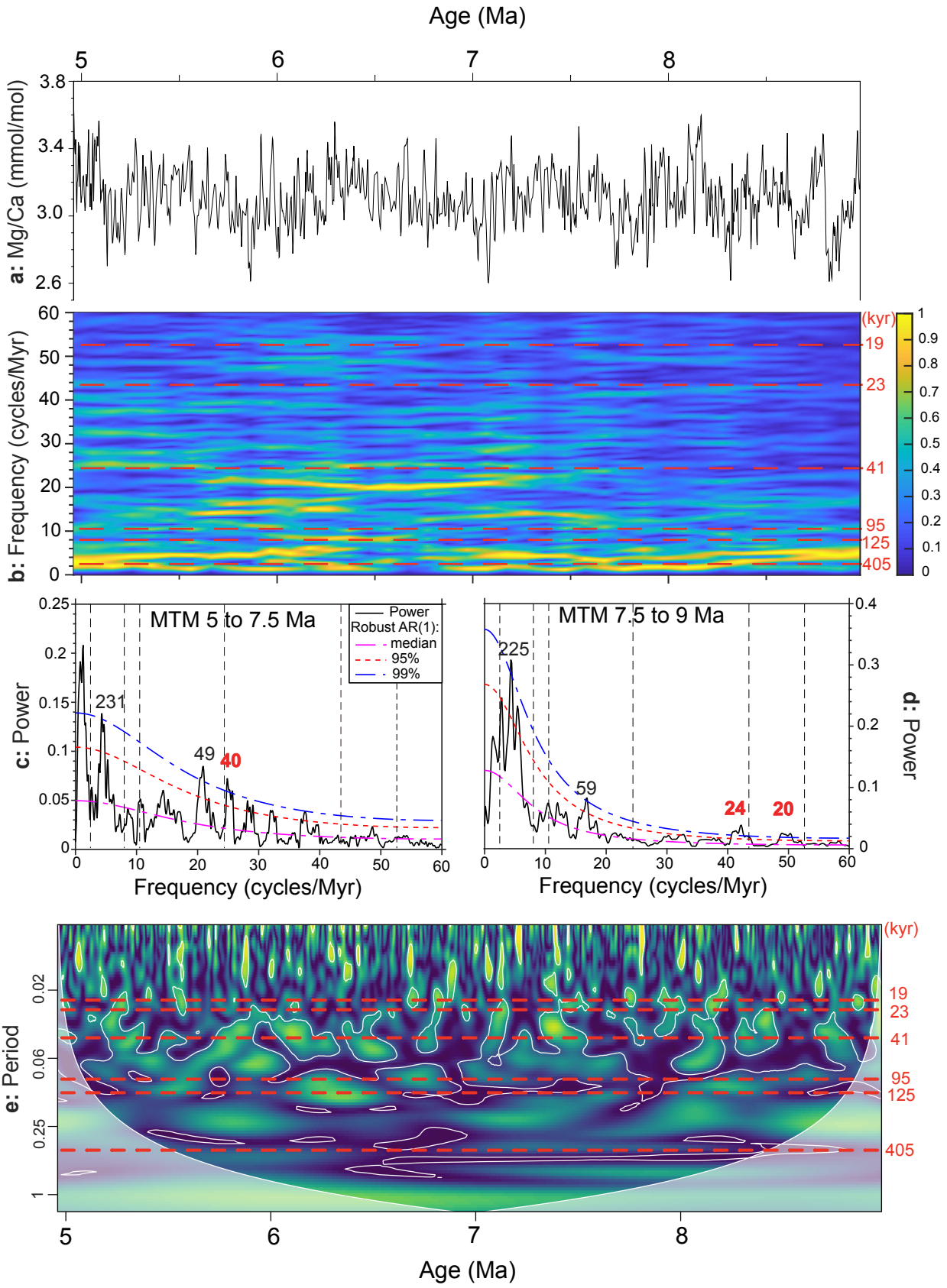
Age (Ma)
a: Mg/Ca (mmol/mol)
b: Frequency (cycles/Myr)
(kyr)
19
23
41
95
125
405
MTM 5 to 7.5 Ma
Power
Robust AR(1):
median
95%
99%
231
49
40
c: Power
Frequency (cycles/Myr)
MTM 7.5 to 9 Ma
225
59
24
20
d: Power
Frequency (cycles/Myr)
e: Period
Age (Ma)

458 **Figure 3.** Time series analyses of Mg/Ca at Site U1443
459 All timeseries analyses were performed on resampled and bandpassed records as described in the
460 methods (a) bandpassed Mg/Ca record (b) evolutive spectral analysis of Mg/Ca, (c) and (d)
461 singular spectral analyses of Mg/Ca over two intervals: from 5 to 7.5 Ma, and from 7.5 to 9 Ma,
462 respectively. (e) Cross-wavelet analyses of Site U1443 Mg/Ca and benthic $\delta^{18}O$. Dashed line on
463 evolutive, spectral and cross-wavelet analyses indicate periods of 404, 124, 95, 41, 24, 22 and 19
464 kyr resulting from Earth's orbital periods. Throughout, primary periods are shown in red and
465 heterodynes in black.

466

467 **5 Discussion**

468 **5.1 Drivers of tropical Indian Ocean SST variability on orbital timescale**

469 Time series analyses of the Site U1443 late Miocene Mg/Ca record reveal a major increase in
470 SST sensitivity to obliquity forcing around 7.5 Ma, at the onset of the LMGC (Figures 3b-d, S7).
471 The appearance of the 49 kyr heterodyne (non-primary orbital period) after 7.5 Ma, alongside an
472 increase in SST variability at the (near-primary) 40 kyr period, could result from the interference
473 of obliquity (41 kyr) and precession (22.4 kyr) periods (Thomas et al., 2016). Before that, from 9
474 to 7.5 Ma, orbital scale SST variability was dominated by precession-band variance (Figure 3d).
475 The influence of precession on tropical Indian Ocean SSTs can be explained either by its direct
476 influence on the seasonal distribution of radiation (Clement et al., 2004), or by its influence on
477 the strength of monsoon winds (e.g., Bosmans et al., 2018), which in turn affect mixed-layer
478 depth and SST (Figure 1). Recent data indicate that no major long-term change in South Asian
479 monsoon wind strength over the equatorial Indian Ocean occurred during the late Miocene
480 (Betzler et al., 2016a, 2018; Bolton et al., 2021), suggesting that an increase in wind-driven
481 mixing is unlikely to have contributed to the cooling trend or to the change in sensitivity of SST
482 to orbital forcing that we document at Site U1443.

483

484 Obliquity cycles are also identified in the ODP Site 1146 Mg/Ca-SST record from the South
485 China Sea, with a similar increase in power after 7.5 Ma (Figure S7; Holbourn et al., 2018). The
486 direct effect of obliquity on low-latitude insolation is small, and the appearance of strong

obliquity cycles in tropical SSTs is broadly concurrent with their appearance in benthic $\delta^{13}C$ and $\delta^{18}O$ from Site U1443 (Bolton et al., 2021) and in a late Miocene benthic $\delta^{18}O$ global stack (Drury et al., 2021), suggesting an increase in tropical SST sensitivity to obliquity linked to an increase in high latitude forcing. Cross-wavelet analysis of SST and benthic $\delta^{18}O$ from Site U1443 show high coherency (>95 %) in the obliquity band (Figure 3e), suggesting that SSTs and deep ocean $\delta^{18}O$ (linked to continental ice volume and temperature in deep-water formation regions) were coupled on orbital timescales during the late Miocene. A number of studies suggest significant changes in cryosphere dynamics during the late Miocene, with the development of ephemeral and dynamic Northern Hemisphere ice sheets (Larsen et al, 1994; Krissek, 1995; Hodell et al., 2001; John & Krissek, 2002; Holbourn et al., 2018; Miller et al. 2020) and Antarctic glacial expansion (Warnke et al., 1992; Ohneiser et al., 2015, Levy et al., 2019). One hypothesis to explain the increased sensitivity to obliquity recorded both in benthic foraminiferal isotopes and in tropical SSTs is that changes in cryosphere dynamics occurring during the LMGC rendered the Earth's climate system more sensitive to obliquity and that feedbacks associated with glacial-interglacial variability also started to affect tropical SSTs after ~7.5 Ma. For the last 0.8 million years, coherence in cyclicity between tropical SSTs and direct measurement of glacial-interglacial variations of atmospheric CO_2 and other greenhouse gases captured in ice cores (Petit et al., 1999; Spahni et al., 2005; Lüthi et al., 2008) support the hypothesis that radiative forcing of atmospheric CO_2 play a dominant role in modulating tropical SST variability on glacial-interglacial timescales (Visser et al. 2003; Lea, 2004; Past Interglacials Working Group of PAGES, 2016). At present, there are no late Miocene pCO_2 reconstructions with a sufficient resolution to allow direct comparison of SSTs and pCO_2 at the glacial-interglacial timescale. In the late Pliocene to early Pleistocene, after the onset of large-scale Northern Hemisphere glaciation at ~2.7 Ma, tropical SSTs are reported to exhibit strong variability on glacial-interglacial timescales, coeval with global climate cycles recorded in benthic $\delta^{18}O$ and pCO_2. Low-latitude SST records show a dominance of 41-kyr cycles before the mid-Pleistocene transition (occurring between 1.2 and 0.6 Ma) and the emergence of 100-kyr cycles during the late Pleistocene (e.g. Liu & Herbert 2004; Liu et al., 2008; Herbert et al., 2010; Li et al., 2011; Li et al., 2017), suggesting "top-down" forcing of tropical SSTs via greenhouse gas forcing. Our late Miocene SST data, considered alongside data from Site 1143 (Holbourn et

al., 2018), suggest that tropical SSTs became more tightly coupled to glacial-interglacial climate and pCO_2 cycles after ~7.5 Ma.

In addition to variability in the obliquity and precession bands, our Mg/Ca-based SST record show variability at the ~400 kyr period (Figure 3b and d; 95 % coherency), which could result from the influence of long eccentricity cycles or the modulation of precession by eccentricity. A number of other studies have recorded ~400 kyr cyclicity in Plio-Pleistocene tropical SSTs (Gupta et al., 1996; Lawrence et al., 2006; Herbert et al, 2010; Li et al, 2011; Li et al., 2017), but the mechanisms involved remain unclear. In one study from the South China Sea, ~400-kyr cycles in SST were suggested to be related to the modulation of the East Asian winter monsoon by El Nino-Southern Oscillation (Li et al., 2017). The presence of ~225 kyr cycles, with two well-defined cycles visible in the oldest part of the Site U1443 SST record between 9 and 8.6 Ma (Figures 2-5) could either represent a real cycle in eccentricity (Hilgen et al., 2020) or a harmonic of the influence of long-eccentricity cycles.

5.2 Late Miocene tropical sea surface cooling

Our new open-ocean tropical Indian Ocean SST record documents a late Miocene cooling of 3.2 °C starting at 7.4 Ma and culminating in minimum temperatures from 6.2 to 5.8 Ma. Following this, a warming of ~1 °C occurs into the early Pliocene (Figures 2, 4 and 5). These broad trends and timings are coherent with stacked $U^{k'}_{37}$-SSTs, although Herbert et al. (2016) record tropical cooling not exceeding 1.5 °C (Figure 4a). SSTs in Eastern Equatorial Pacific (EEP) ODP Site 850 and in West Pacific Warm Pool (WPWP) ODP Site 806 reconstructed with the TEX_{86} index (Zhang et al., 2014) record ~2 °C and 1.5 °C of cooling from 7.5 to 5 Ma, respectively, whereas TEX_{86}-SSTs at ODP Site 1143 in the South China Sea (Zhang et al., 2014) show a <1 °C cooling over the same period (Figure S8b). The three tropical sites where SSTs were reconstructed using *T. trilobus* Mg/Ca ratios (Figure 5a-c) show broadly similar long-term trends, although the amplitude of SST changes and exact timings are variable. The less pronounced late Miocene cooling trend in all $U^{k'}_{37}$ and some TEX_{86} records compared to Mg/Ca-SSTs from Site U1443 may stem from proxy biases (discussed in section 5.2.1), aliasing due to the low resolution of

many records, and/or errors related to the use of shipboard biostratigraphy and magnetostratigraphy for age control.

A driver of documented global sea surface cooling could be a decrease in pCO_2. Indeed, while certain late Miocene pCO_2 reconstructions based on carbon isotopic fractionation ($\delta^{13}C$) in alkenones (Pagani et al., 1999, 2005; Zhang et al., 2013), leaf stomata (Kürschner et al., 1996; Retallack, 2009; Stults et al 2011), and planktic foraminiferal boron isotopes ($\delta^{11}B$) (Sosdian et al., 2018) suggested relatively constant pCO_2 close to preindustrial values (~250-350 ppm), a number of recent studies that include higher-resolution sampling and/or new interpretive frameworks now point towards higher Miocene pCO_2 and a significant decrease over the late Miocene (Brown et al., in review; Bolton et al., 2016; Mejia et al., 2017; Stoll et al 2019; Tanner et al., 2020; see also the review and revision of published pCO_2 data in Rae et al., 2021). For instance, studies based on marine phytoplankton $\delta^{13}C$ suggest a pCO_2 decrease from between 800 and 560 ppm at 7.5 Ma to ~350 to 300 ppm at 5 Ma (Mejia et al., 2017, Tanner et al., 2020). Indirect evidence from the $\delta^{13}C$ composition of coccoliths, arising about 7 to 5 Ma ago and interpreted as a threshold response of cells to decreasing aqueous CO_2 concentrations, also strengthens the hypothesis of declining pCO_2 during the late Miocene (Bolton & Stoll, 2013).

Therefore, considering a pCO_2 range in agreement with available proxy reconstructions (Figure 4b), we used late Miocene paleoclimate simulations under three atmospheric pCO_2 scenarios to test if a pCO_2 decrease may have driven global sea surface cooling over the late Miocene, and to estimate how much of the 3.2 °C tropical SST cooling observed at Site U1443 could be explained by pCO_2 forcing. In the following we compare compiled global SSTs at 8 ±0.5 Ma and at 6 ±0.5 Ma (see section 3.4) with SSTs simulated at 300 ppm (LM-300), 420 ppm (LM-420) and 560 ppm (LM-560) (Figures 6-7).

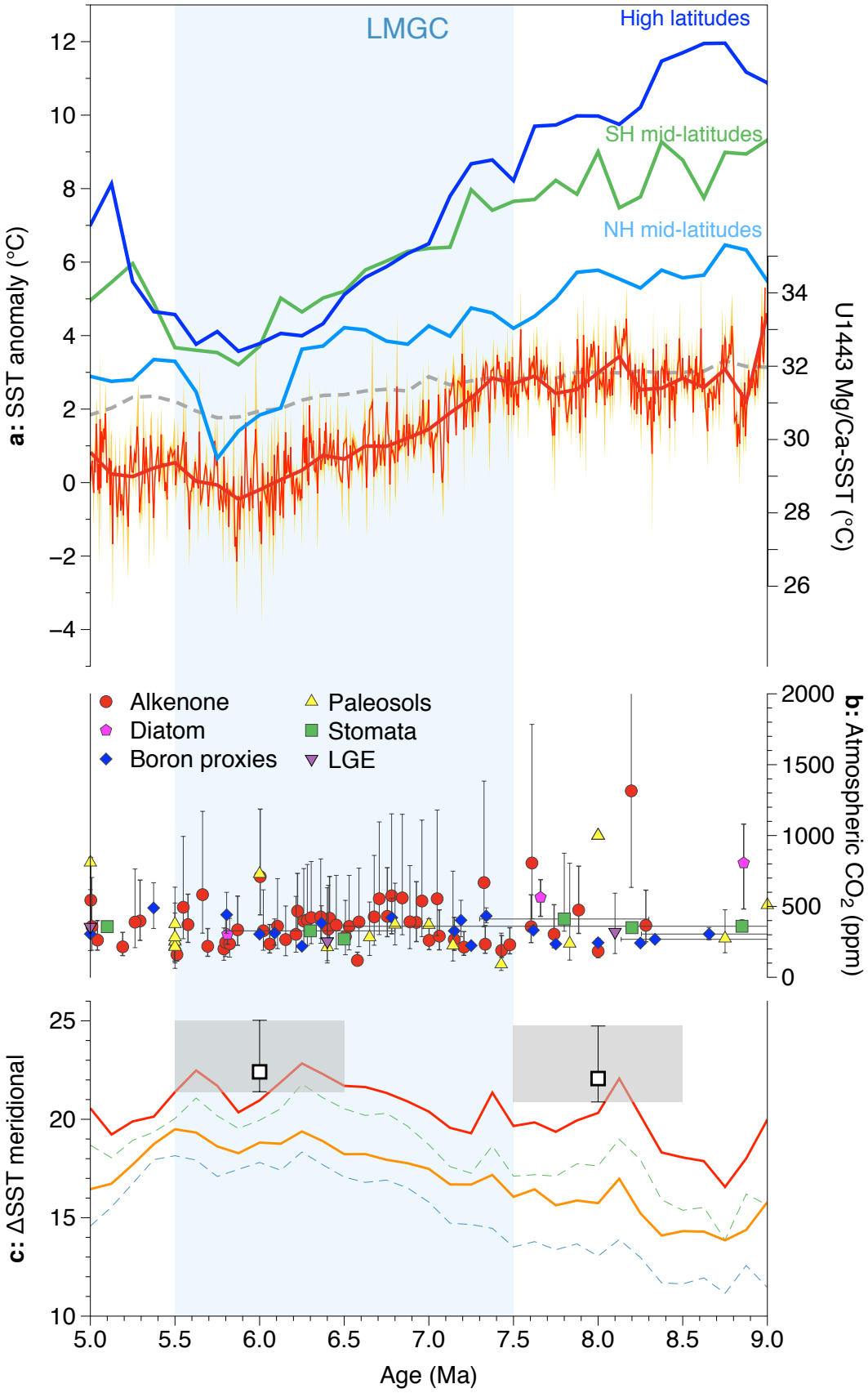
LMGC
High latitudes
SH mid-latitudes
NH mid-latitudes
a: SST anomaly (°C)
U1443 Mg/Ca-SST (°C)
Alkenone
Diatom
Boron proxies
Paleosols
Stomata
LGE
b: Atmospheric CO2 (ppm)
c: ΔSST meridional
Age (Ma)

572 **Figure 4**. Late Miocene global cooling, pCO_2 proxy data, and evolution of latitudinal thermal
573 gradients. (a) Stacked SST anomalies based on $U^{K'}_{37}$ data for the tropics (grey curve), mid-
574 latitudes (green and blue curves) and high northern latitudes (dark blue curve) from Herbert et al.
575 (2016), with new U1443 Mg/Ca-SST (red curve). All data are shown as SST anomalies relative
576 to the modern (left axis) and absolute SST values for Site U1443 are also shown (right axis). (b)
577 Late Miocene pCO_2 proxy data compilation obtained from https://paleo-co2.org with data from
578 Mejia et al., 2017, Tanner et al., 2020 and Rae et al., 2021 added. (c) Evolution of latitudinal
579 SST gradients between Northern Hemisphere high latitudes and tropics. Red and orange curves
580 are calculated using U1443 Mg/Ca-SST as representative of the tropical trend minus the
581 Northern Hemisphere high latitude $U^{K'}_{37}$-SST stack (Sites 883/884, 887, 907 and 982) (orange
582 curve) and the $U^{K'}_{37}$-SST stack without North Atlantic Site 982 (red curve). Green and blue
583 dashed curves are calculated using the $U^{K'}_{37}$-SST tropical stack (Sites 722, 846, 850, 1241,
584 U1338) minus Northern Hemisphere high latitudes $U^{K'}_{37}$-SST stack (green dashed curve) and
585 $U^{K'}_{37}$-SST stack without North Atlantic Site 982 (blue dashed curve). Squares represent values of
586 modelled latitudinal SST gradients at 8 ±0.5 Ma and 6 ±0.5 Ma corresponding to LM-560 and
587 LM-300 simulations, respectively, using the mean annual SST average over the entire latitude
588 band between 5°S and 19°N for the tropics and 48°N and 70°N for the high latitudes (see section
589 5.2.3).

590

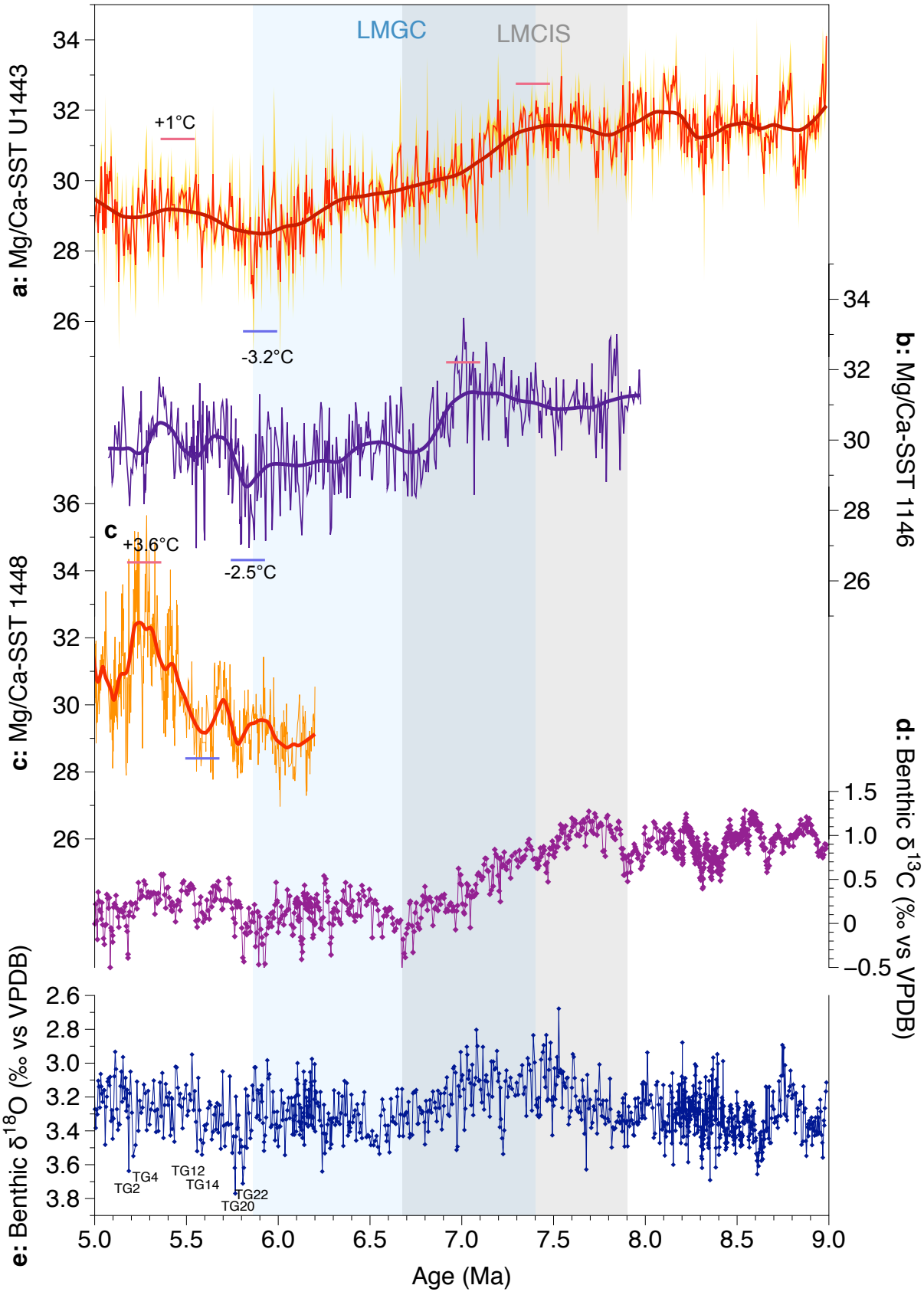
LMGC
LMCIS
+1°C
-3.2°C
a: Mg/Ca-SST U1443
b: Mg/Ca-SST 1146
c
+3.6°C
-2.5°C
c: Mg/Ca-SST 1448
d: Benthic δ13C (‰ vs VPDB)
e: Benthic δ18O (‰ vs VPDB)
TG2
TG4
TG12
TG14
TG20
TG22
Age (Ma)

591

592 **Figure 5.** Tropical high-resolution SST records for the late Miocene (9 to 5 Ma).
593 (a) Mg/Ca-SST from equatorial Indian Ocean Site U1443, (b) Mg/Ca-SST from South China Sea
594 Site 1146 (Holbourn et al., 2018) and (c) Mg/Ca-SST from Andaman Sea Site U1448 (Jöhnck et
595 al., 2020). All SST records were recalculated using the same calibration and Mg/Ca_{sw} correction
596 as in Fig. 2., the thick curves are 10 % Lowess filters. (d) Site U1443 benthic (*C. wuellerstorfi*)
597 $\delta^{13}C$ (Bolton et al., 2021) and (e) Site U1443 benthic $\delta^{18}O$ (Bolton et al., 2021) with Thvera-Gilbert
598 (TG) cold stages marked. Blue shading represents the Late Miocene Global Cooling (LMGC)
599 interval and grey shading represent the late Miocene carbon isotope shift (LMCIS).

600

601 **5.2.1 Tropical sea surface temperature records and model results**

602 At 6 ±0.5 Ma, SSTs from the LM-300 simulation fit well with all tropical proxy-derived SSTs
603 (Figure 6a), except two sites that show slightly warmer reconstructed SSTs compared to
604 modelled ones at the same locations; ODP Sites 1146 (Holbourn et al., 2018) and 806 (Zhang et
605 al., 2014) (site locations are shown in Figure 7). Site 1146 in the semi-enclosed South China Sea
606 is under the influence of the East Asian monsoon subsystem, and the stepwise cooling in Mg/Ca-
607 SSTs at 6.8 Ma (Figure 5b) has been attributed to a southward shift of the Intertropical
608 Convergence Zone linked to cooling of the Northern Hemisphere and a consequent change in
609 monsoon regime (Holbourn et al., 2018). At Site 806 in the WPWP, TEX_{86}-SSTs are above 28
610 °C for the entire record (Zhang et al., 2014), coherent with expected SSTs for warm pool regions
611 (e.g. Vinayachandran & Shetye, 1991; Yan et al., 1992). However, Site 806 is thought to record
612 the Miocene evolution of the proto-WPWP, forced by tectonic constriction of the Indonesian
613 Gateway and eustatic fluctuations (Kuhnt et al., 2004; Sosdian & Lear, 2020), potentially
614 affecting SST trends (e.g. Nathan & Leckie, 2009; Sosdian & Lear, 2020). Therefore, additional
615 regional influences at these two sites could explain the discrepancies between modelled and
616 reconstructed SSTs (Figure 6a). The LM-300 simulation also shows good agreement with SST
617 data at 6 ±0.5 Ma in mid and high latitudes, except in the North Atlantic Ocean and one site in
618 the South Pacific (Figure 6a). The discrepancy between proxy- and model-derived SSTs in the
619 North Atlantic is a systematic bias in paleoclimate modelling studies (e.g. Dowset et al., 2013;
620 Burls et al. 2021) and is present in all our simulations (see section 5.2.3).

621

We next compared compiled SST data at 8 ±0.5 Ma to SSTs in LM-300, LM-420 and LM-560 simulations (Figure 6b). SSTs from the LM-300 simulations are too low compared to proxy-derived SSTs from all latitudes, with the exception of TEX_{86}-SSTs from the EEP cold tongue and from the South China Sea (Sites 850 and 1143, respectively, Zhang et al., 2014) . SSTs from the LM-560 and LM-420 simulations show good agreement with SST data at 8 ±0.5 Ma for mid and high latitudes (excluding the North Atlantic Ocean) but differ in the tropics. SSTs in LM-560 fit well with tropical Mg/Ca-SSTs from Site U1443 and TEX_{86}-SSTs from Site 806, but are warmer than tropical $U^{k'}_{37}$-SSTs (Figure 6b). Conversely, SSTs in the LM-420 simulation show better agreement with tropical $U^{k'}_{37}$-SSTs but are cooler than Site U1443 Mg/Ca-SST and Site 806 WPWP records (Figure 6b). TEX_{86}-SSTs from the EEP (Site 850) and the South China Sea (Site 1143) are cooler than in the LM-420 and LM-560 simulations.

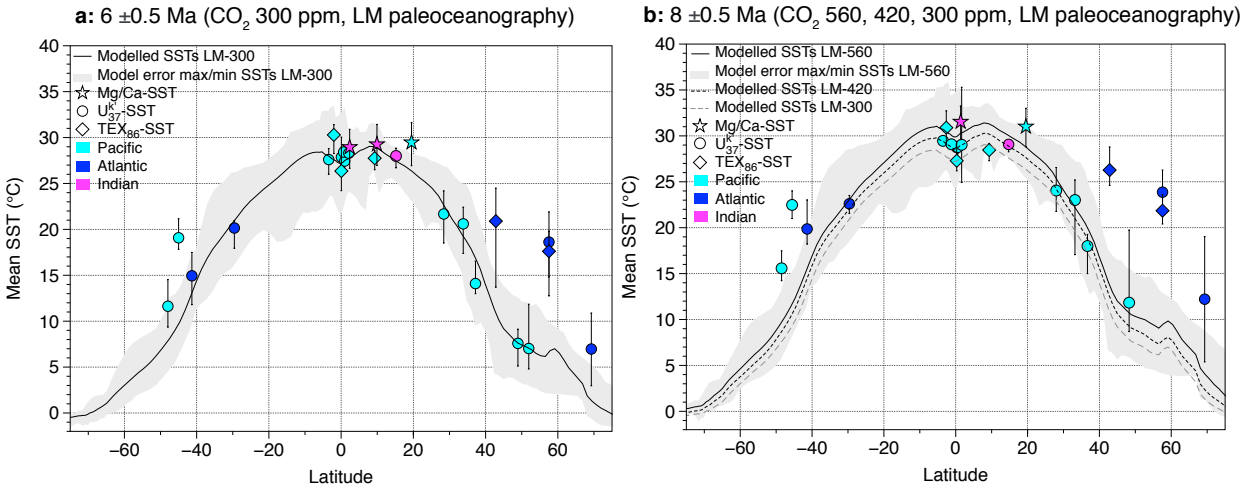

Figure 6. Mean modelled latitudinal SST gradients and proxy-derived SSTs.
The LM-560 simulation (b) and LM-300 simulation (a) correspond to atmospheric CO_2 fixed at 560 ppm and 300 ppm, respectively, under late Miocene boundary conditions (see methods). In panel (b), LM-420 and LM-300 simulations are also shown with black and grey dashed lines, respectively. LM-560 and LM-300 simulations are compared to our global SST compilation from proxies (Mg/Ca, $U^{K'}_{37}$ and TEX_{86}) in 1 Myr time windows centered on 8 Ma and 6 Ma, respectively. The grey envelope represents maximum and minimum mean annual SSTs at each latitude. All proxy-derived SSTs were recalculated in a consistent way (see Methods) and are

plotted at their paleolatitude at 8 and 6 Ma (PaleoAtlas for Gplates, Scotese, 2016). In brief, Mg/Ca SSTs were recalculated as in Fig. 2 and 4, $U^{K'}_{37}$ SSTs were recalculated using the BAYSPLINE calibration (Tierney & Tingley, 2018), and TEX_{86} SST were recalculated using the BAYSPAR Analog mode calibration (Tierney & Tingley, 2015).

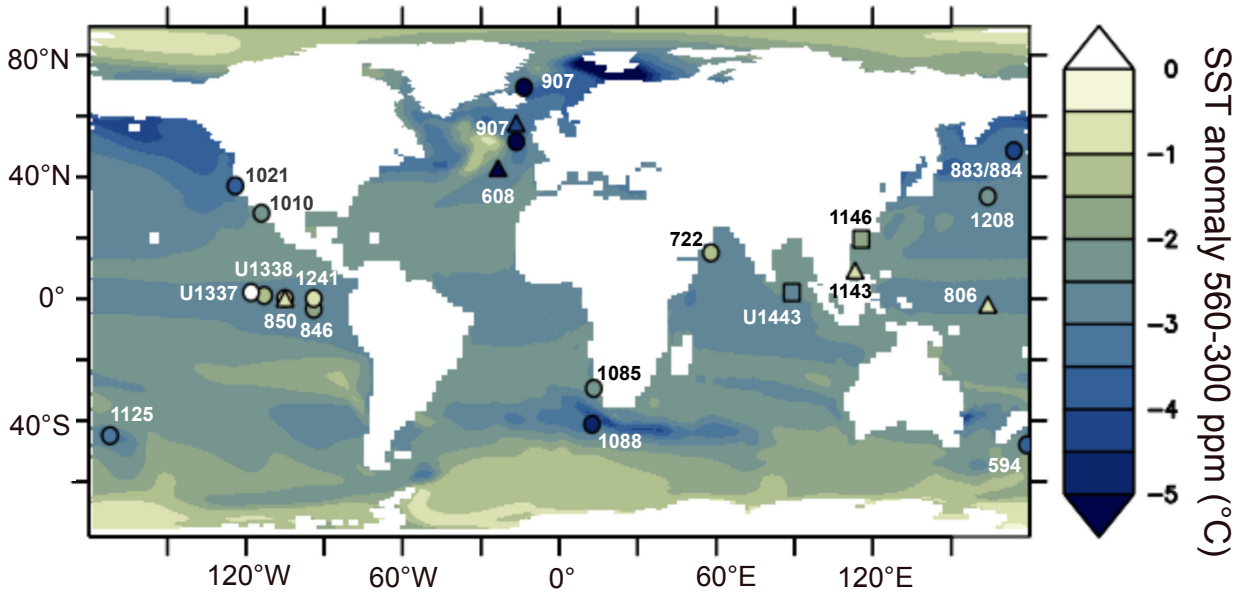

Figure 7. Model-data comparison of the amplitude of the late Miocene cooling. The map background color scale shows the SST anomaly from the LM-560 simulation minus the LM-300 simulation and indicates the amplitude of modelled late Miocene cooling that best fits with proxies-derived SSTs. Sites with available late Miocene SST records (symbols) are placed on the map at their average paleolocation between 8 and 6 Ma (paleolocation from PaleoAtlas for Gplates, Scotese, 2016). The amplitude of SST cooling based on site-specific proxy records (colour within symbols) is calculated from averaged SSTs at 8 ±0.5 Ma minus 6 ±0.5 Ma. Squares indicate Mg/Ca-SST records, triangles indicate TEX_{86}-SST records and circles indicate $U^{k'}_{37}$-SST records. All SSTs were recalculated in a consistent way as described in the caption of Figure 6. The same color scale is used for the map background and in the symbols.

A number of studies have demonstrated the limitations of alkenone paleothermometry for reconstructing SSTs in warm waters. The first concerns the application of a classical linear calibration (e.g. Prahl et al., 1988; Müller et al., 1998) that results in underestimation of temperatures >24 °C (e.g. Goni et al., 2001; Richey & Tierney, 2016). For this reason, we

664 recalculated all $U^{k'}_{37}$-SSTs with the updated BAYSPLINE calibration (Tierney & Tingley, 2018).
665 Another limitation concerns the difficulty of measuring very low concentrations of tri-
666 unsaturated C_{37} alkenones in sediments when the $U^{k'}_{37}$ index approaches its limit of 1, indicative
667 of temperatures higher than 28 °C (Grimalt et al., 2001; Pelejero & Calvo, 2003; Richey &
668 Tierney, 2016). Because of this, all published tropical $U^{k'}_{37}$-SST records come from sites located
669 in upwelling regions. Arabian Sea ODP Site 722 is located in a coastal upwelling region forced
670 by the southwest winds of the South Asian summer monsoon. Other sites (ODP Sites 846, 850,
671 U1338 and 1241) are located in the EEP. Sites 846, 850 and U1338 are under the influence of
672 cold tongue upwelling or equatorial divergence and Site 1241 is out of the upwelling centre
673 today but was located further south, closer to the equatorial divergence, during the late Miocene
674 (Mix et al., 2003). However, in all of these sites, in sediments older than 6.5 to 7 Ma, the $U^{k'}_{37}$
675 index approaches its limit of 1 ($U^{k'}_{37}$ = 0.96 to 0.99). This could provide an explanation for the
676 lower tropical SSTs derived from the $U^{k'}_{37}$ index before 6.5 Ma, and therefore for the less
677 pronounced tropical cooling in $U^{k'}_{37}$ records during the LMGC (on the order of 1-2 °C when
678 recalculated with BAYSPLINE calibration; Figures 7 and S8a) compared to cooling from
679 Mg/Ca-SST and from modelled SST (Figures 6-7). Moreover, these upwelling systems in the
680 EEP and Arabian Sea are dynamic and their strength depends both on oceanographic and
681 paleogeographic constraints, with significant changes suggested for the Miocene (Holbourn et
682 al., 2014; Tian et al., 2014; Zhang et al., 2014; Gupta et al. 2015; Zhuang et al. 2017; Bialik et
683 al., 2020; Sarr et al. in review). Thus, it is difficult to decouple the impact of changes in
684 upwelling strength on SSTs from global SST trends at these sites.

685

686 TEX_{86}-SSTs reconstructed at ODP Site 850 (Zhang et al., 2014) record very variable
687 temperatures from 9 to 5 Ma comprised between 21 and 32 °C with minimum temperatures
688 between 5.5 and 5 Ma (21 to 23 °C), whereas $U^{k'}_{37}$-SSTs from the same site are less variable
689 between 27.5 and 29 °C (Figure S8). In the modern ocean, ODP Site 850 is located in the EEP
690 cold tongue, characterized by a shallow thermocline and intense upwelling. One plausible
691 explanation for this discrepancy between TEX_{86} and $U^{k'}_{37}$ temperatures could be that the TEX_{86}
692 paleothermometer records a depth-integrated signal rather than a surface one, as many studies
693 have reported that GDGT producers can inhabit a large vertical range in the water column (e.g.
694 Lipp & Hinrichs, 2009; Ho & Laepple, 2015, 2016; Richey & Tierney, 2016; Leduc et al., 2017;

695 Van der Weijst et al., 2021). Given the potential underestimation of tropical $U^{k'}_{37}$-SST before
696 ~6.5 Ma and the possibility that TEX_{86} temperatures recorded at Sites 850 represent cooler
697 subsurface waters, we think that the LM-560 scenario shows the best fit with SST data for 8 ±0.5
698 Ma.

699

700 **5.2.2 pCO_2 as a primary driver of late Miocene cooling**

701 In light of our data-model comparison, and considering our new tropical SST record and recent
702 advances in pCO_2 estimates, we consider that the most likely scenario for late Miocene pCO_2
703 evolution is represented by a decrease from 560 ppm around 8 Ma to 300 ppm around 6 Ma at
704 the end of the LMGC. In the vicinity of Site U1443, simulated SSTs are 32 to 32.5 °C in the LM-
705 560 simulation (interpreted as representative of ~8 Ma) and 29.5 to 30 °C in the LM-300
706 simulation (representative of ~6 Ma) (Figure S9) implying that 2 to 3 °C of sea surface cooling
707 can be explained by atmospheric pCO_2 decrease and associated atmosphere-ocean feedbacks.
708 This represent 63 to 94 % of the total late Miocene SST cooling (3.2 °C) estimated at Site
709 U1443, corroborating the hypothesis that long-term SST evolution at this location is relatively
710 insulated from local processes and is representative of global low-latitude trends over the late
711 Miocene. Our new tropical SST record significantly increases previous estimates of tropical
712 cooling during the late Miocene, with implications for estimates of climate sensitivity (to date
713 based on tropical $U^{k'}_{37}$-SSTs; Brown et al., in review) and the evolution of meridional thermal
714 gradients (Herbert et al., 2016). Nevertheless, based on the results of our pCO_2 simulations, up to
715 a third of the late Miocene cooling estimated for the equatorial Indian Ocean could be linked to
716 other (presumably regional) phenomena, discussed below.

717

718 Extension of the Antarctic ice sheet during the late Miocene could have influenced water mass
719 properties in deep-water formation regions, which in turn could have impacted low-latitude
720 surface waters via plumbing to upwelling regions (Warnke et al., 1992; Ohneiser et al., 2015,
721 Levy et al., 2019); however, this mechanism is unlikely to have contributed to SST cooling at
722 Site U1443. On the other hand, regional tectonic activity (the collision of Australia and eastern
723 Indonesia since the early Miocene, progressive constriction and shoaling of Indonesian

724 Gateway), and glacio-eustatic sea level fluctuations that affected the geometry of the Indonesian
725 Gateway and ITF (e.g. Kuhnt et al., 2004; Hall et al., 2009; Molnar & Cronin, 2015; Sosdian &
726 Lear, 2020) could have influenced regional SSTs during the late Miocene. In the modern, warm,
727 fresh waters flowing from the Pacific into the Indian Ocean via the ITF contribute significantly
728 to intermediate water masses that occupy the Indian Ocean thermocline (You & Tomczak, 1993;
729 Gordon & Fine, 1996; Tomczak & Godfrey, 2001; Gordon, 2005). Our late Miocene simulations
730 do not account for any potential paleogeographic or ITF changes coeval with the LMGC,
731 because the model resolution is insufficient to allow us to reconstruct the complex geography of
732 the Indonesian Gateway area. Previous modelling studies however suggest that an ITF restriction
733 could generate a 2 to 3 °C cooling of surface and subsurface waters in the eastern Indian Ocean
734 (Cane & Molnar 2001; Krebs et al., 2011). Although the exact timing of the gateway constriction
735 is still poorly constrained, with estimates ranging from ~17 Ma to 4 to 3 Ma (e.g. Kennett et al.,
736 1985; Hodell & Vayavananda, 1993; Hall et al, 1988, 2002,2012; Kuhnt et al.,2004; Li et al.,
737 2006; Gallagher et al. 2009, Nathan & Leckie, 2009), late Miocene changes related to tectonic
738 activity and/or sea-level drop linked to Antarctic glaciation remains one plausible mechanisms
739 for amplification of cooling magnitude in the equatorial Indian Ocean (Site U1443). Additional
740 late Miocene SST and other proxy records from the Australian Shelf and Timor Sea are needed
741 to allow precise reconstruction of the timing of late Miocene ITF restriction, and to gain a better
742 understanding of the effect of these changes on Indian Ocean SSTs.

743

744 **5.2.3 Extratropical sea surface temperatures and late Miocene evolution of meridional**
745 **gradients**

746 In our data-model comparison, proxy-derived extratropical SSTs at 8 ±0.5 Ma and at 6 ±0.5 Ma
747 show good agreement with modelled SSTs from our preferred scenario (pCO_2 decrease from 560
748 ppm to 300 ppm) both in term of absolute temperature and amplitude of cooling (Figures 6 and
749 7) except for the North Atlantic Ocean where proxy-derived SSTs are always warmer than
750 modelled SSTs (Figure 6). This feature is a systematic bias in paleoclimate modelling studies
751 that generally fail to reproduce estimated latitudinal temperature gradients (e.g. Dowset et al.,
752 2013; Burls et al., 2021). Temperature biases are often attributed to poor representation of cloud
753 microphysics and/or to a lack of cloud-aerosol interaction in state-of the art climate models

(Burls et al., 2021; Zhu et al., 2019), although Otto-Bliesner et al. (2017) also suggest that the failure to reproduce warm North Atlantic SSTs in Pliocene simulations (Dowsett et al. 2013) could be attributed to the inexact representation of Arctic gateways that are crucial for the simulation of Atlantic Meridional Overturning Circulation and North Atlantic climate sensitivity. In addition, Mejia et al. (2020) recently used clumped isotope temperature data to argue that the amplitude of late Miocene North Atlantic $U^{k'}_{37}$-SST cooling may have been overestimated due to seasonal bias in alkenone production.

Keeping in mind the potential biases in North Atlantic SST estimates and based on the assumption that SSTs from Site U1443 are representative of global low-latitude trends over the late Miocene, we estimate the evolution of proxy-derived meridional SST gradients and compare this to simulated meridional SST gradients. To calculate model-derived gradients, we averaged mean annual SSTs over the entire latitudinal band between 5 °S and 19 °N for the tropics and 48 °N and 70 °N for the northern high latitudes in the LM-560 and LM-300 simulations to represent condition at 8 ±0.5 Ma to 6 ±0.5 Ma, respectively. These latitudinal bands correspond to the regions covered by proxies-derived SST records used to estimate meridional gradients, taking into account their late Miocene paleolocations (Figure 7). To calculate proxy-derived meridional SST gradient evolution, we used the difference between tropical Mg/Ca-SST at Site U1443 and Northern Hemisphere high-latitude stacked $U^{k'}_{37}$-SST including the four sites in Herbert et al. (2016) (Figure 4c orange curve) and excluding North Atlantic ODP Site 982 where reconstructed $U^{k'}_{37}$-SSTs are particularly warm (mean value of 21.6 °C between 9 and 5 Ma) (Figure 4c red curve). From 8 ±0.5 Ma to 6 ±0.5 Ma, the data-based meridional gradient shows a 3.3 °C (2 °C) increase, depending on the inclusion (exclusion) of Site 982 in the northern high-latitude $U^{k'}_{37}$-SST stack. In comparison, when tropical stacked $U^{k'}_{37}$-SSTs are used in the calculation instead of U1443 Mg/Ca-SSTs, a much higher increase in meridional gradient of 4.6 °C (3.3 °C) is suggested, again dependant on the inclusion (exclusion) of Site 982 (Figure 5c dashed curves). On the other hand, simulated meridional SST gradients do not show a significant increase from 8 to 6 Ma and have a value of ~22 °C. This comparison reveals that estimations of meridional SST gradient evolution over the late Miocene using Site U1443 Mg/Ca-SST to represent the global low-latitude trend and stacked $U^{k'}_{37}$-SST (excluding North Atlantic Site 982) to represent the global Northern Hemisphere high-latitude trend result in a much better data-model agreement

(Figure 4c). These finding suggest that the choice of sites adapted to register global latitudinal trends and the choice of proxies adapted to reconstruct mean annual SST are crucial and could explain in part the discrepancies often observed between proxy- and model-derived SSTs and resultant estimates of meridional temperature gradients. These new results suggest a much more modest increase in meridional SSTs gradients during the LMGC than previously suggested by $U^{k'}_{37}$-SSTs stacks, with important implication regarding our comprehension of the late Miocene climate system (for example, estimations of polar amplification and the strength of atmospheric circulation and Hadley cells).

6 Conclusions

We present a new orbital-resolution equatorial Indian Ocean Mg/Ca-SST record spanning the interval from 9 to 5 Ma (late Miocene-earliest Pliocene) together with new late Miocene climate simulations under three pCO_2 scenarios (300 ppm, 420 ppm and 560 ppm, in the range of pCO_2 proxy reconstructions). To date, this is the first late Miocene tropical SST record located in an open-ocean region with sufficient resolution to also resolve orbital scale variability. Our record shows a tropical SST cooling of 3.2 °C from 7.4 Ma until 5.8 Ma, similar in magnitude and timing to previously published mid-latitude $U^{k'}_{37}$-SST trends. Our data-model comparison supports the hypothesis that a pCO_2 decrease from around 560 ppm before the LMGC to around 300 ppm at the end of the LMGC may have driven global SST cooling, consistent with recent revised and new pCO_2 reconstructions (Brown et al., in review; Mejia et al., 2017; Rae et al., 2021; Tanner et al., 2020) and with the pCO_2 decrease hypothesised in Herbert et al. (2016). pCO_2 forcing of SST can explain over two thirds of the cooling trend at Site U1443. In addition, time series analyses reveal a major increase in tropical (Sites U1443 and 1146) SST sensitivity to obliquity forcing at the onset of the LMGC, suggesting that tropical SSTs became more tightly coupled to glacial-interglacial climate during this time. Together, these results support the hypothesis that the late Miocene underwent a secular decrease in tropical SST mostly driven by atmospheric pCO_2 decrease, but with a much more modest increase in meridional SST gradients than previously suggested**.**

Acknowledgments

The authors declare that they have no conflict of interest. This research used samples provided by the International Ocean Discovery Program (IODP). We thank the science party, technical staff and crew of IODP Expedition 353 (Indian Monsoon Rainfall); and the CEA–CCRT for providing access to the HPC resources of TGCC under the allocation 2019-A0070102212 made by GENCI. Lyndsey Fox is thanked for sharing taxonomic expertise. Funding for this research was provided by French ANR projects iMonsoon ANR-16-CE01-0004-01 (CTB) and AMOR ANR-16-CE31-0020 (YD), IODP France post-cruise funding (CTB), and a French Ministerial PhD scholarship awarded to C.M. C.M., C.T.B., K.T and A.C.S. designed the study. Sample processing was carried out by C.T.B and E.G. Picking and cleaning of planktic foraminifera was carried out by C.M and E.G. ICP-MS analyses were performed by M.G., and model simulations were performed by A.C.S. with Y.D. C.M. wrote the manuscript with contributions and feedback from C.T.B, K.T., A.C.S and Y.D.

Open Research

All data are archived at www.pangaea.de (submitted 19.11.2021, awaiting validation)

References

Allen, K. A., Hönisch, B., Eggins, S. M., Haynes, L. L., Rosenthal, Y., & Yu, J. (2016). Trace element proxies for surface ocean conditions: A synthesis of culture calibrations with planktic foraminifera. *Geochimica et Cosmochimica Acta*, *193*, 197-221. https://doi.org/10.1016/j.gca.2016.08.015

Anand, P., Elderfield, H., & Conte, M. H. (2003). Calibration of Mg/Ca thermometry in planktonic foraminifera from a sediment trap time series. *Paleoceanography*, *18*(2). https://doi.org/10.1029/2002PA000846

Andrae, J. W., McInerney, F. A., Polissar, P. J., Sniderman, J. M. K., Howard, S., Hall, P. A., & Phelps, S. R. (2018). Initial expansion of C4 vegetation in Australia during the late Pliocene. *Geophysical Research Letters*, *45*(10), 4831-4840. https://doi.org/10.1029/2018GL077833

Aumont, O., Éthé, C., Tagliabue, A., Bopp, L., & Gehlen, M. (2015). PISCES-v2: an ocean biogeochemical model for carbon and ecosystem studies. *Geoscientific Model Development*, *8*(8), 2465-2513. https://doi.org/10.5194/gmd-8-2465-2015

Bailey, I., Foster, G. L., Wilson, P. A., Jovane, L., Storey, C. D., Trueman, C. N., & Becker, J. (2012). Flux and provenance of ice-rafted debris in the earliest Pleistocene sub-polar North Atlantic Ocean comparable to the last glacial maximum. *Earth and Planetary Science Letters*, *341*, 222-233. https://doi.org/10.1016/j.epsl.2012.05.034

Balco, G., & Rovey, C. W. (2010). Absolute chronology for major Pleistocene advances of the Laurentide Ice Sheet. *Geology*, *38*(9), 795-798. https://doi.org/10.1130/G30946.1

Barker, S., Greaves, M., & Elderfield, H. (2003). A study of cleaning procedures used for foraminiferal Mg/Ca paleothermometry. *Geochemistry, Geophysics, Geosystems*, *4*(9). https://doi.org/10.1029/2003GC000559

Bassinot, F. C., Beaufort, L., Vincent, E., Labeyrie, L. D., Rostek, F., Müller, P. J., ... & Lancelot, Y. (1994). Coarse fraction fluctuations in pelagic carbonate sediments from the tropical Indian Ocean: A 1500-kyr record of carbonate dissolution. *Paleoceanography*, *9*(4), 579-600. https://doi.org/10.1029/94PA00860

Bé, A.W.H. (1980). Gametogenic calcification in a spinose planktonic foraminifer, Globigerinoides sacculifer (Brady).*Marine Micropaleontology*, *5*, 283-310. https://doi.org/10.1016/0377-8398(80)90014-6

Bé, A.W.H., and Tolderlund, D.S., (1971). Distribution and ecology of living planktonic foraminifera in surface waters of the Atlantic and Indian Oceans: *in* Funnell, W. R., and Riedel, W. R. (eds.), The Micropaleontology of Oceans, Cambridge University Press, New York, p. 105-149.

875 Beerling, D. J., & Royer, D. L. (2011). Convergent cenozoic CO2 history. *Nature*
876 *Geoscience*, *4*(7), 418-420. https://doi.org/10.1038/ngeo1186
877 Berner, R. A. (2004). A model for calcium, magnesium and sulfate in seawater over Phanerozoic
878 time. *American Journal of Science*, *304*(5), 438-453. https://doi.org/10.2475/ajs.304.5.438
879
880 Betzler, C., Eberli, G. P., Kroon, D., Wright, J. D., Swart, P. K., Nath, B. N., ... & Young, J. R.
881 (2016). The abrupt onset of the modern South Asian Monsoon winds. *Scientific reports*, *6*(1), 1-
882 10. https://doi.org/10.1038/srep29838
883
884 Betzler, C., Eberli, G. P., Lüdmann, T., Reolid, J., Kroon, D., Reijmer, J. J. G., ... & Yao, Z.
885 (2018). Refinement of Miocene sea level and monsoon events from the sedimentary archive of
886 the Maldives (Indian Ocean). *Progress in Earth and Planetary Science*, *5*(1), 1-18.
887 https://doi.org/10.1186/s40645-018-0165-x
888
889 Bialik, O. M., Auer, G., Ogawa, N. O., Kroon, D., Waldmann, N. D., & Ohkouchi, N. (2020).
890 Monsoons, upwelling, and the deoxygenation of the northwestern Indian Ocean in response to
891 middle to late Miocene global climatic shifts. *Paleoceanography and Paleoclimatology*, *35*(2).
892 https://doi.org/ 10.1029/2019PA003762
893
894 Bolton, C. T., Gray, E., Kuhnt, W., Holbourn, A. E., Lübbers, J., Grant, K., ... & Andersen, N.
895 (2021). Secular and orbital-scale variability of equatorial Indian Ocean summer monsoon winds
896 during the late Miocene. *Climate of the Past Discussions*, 1-45. https://doi.org/10.5194/cp-2021-
897 77
898
899 Bolton, C. T., Hernández-Sánchez, M. T., Fuertes, M. A., González-Lemos, S., Abrevaya, L.,
900 Mendez-Vicente, A., ... & Stoll, H. M. (2016). Decrease in coccolithophore calcification and
901 CO2 since the middle Miocene. *Nature communications*, *7*(1), 1-13.
902 https://doi.org/10.1038/ncomms10284
903
904 Bolton, C. T., & Stoll, H. M. (2013). Late Miocene threshold response of marine algae to carbon
905 dioxide limitation. *Nature*, *500*(7464), 558-562. https://doi.org/10.1038/nature12448

Bosmans, J. H. C., Erb, M. P., Dolan, A. M., Drijfhout, S. S., Tuenter, E., Hilgen, F. J., ... & Lourens, L. J. (2018). Response of the Asian summer monsoons to idealized precession and obliquity forcing in a set of GCMs. *Quaternary Science Reviews*, *188*, 121-135. https://doi.org/10.1016/j.quascirev.2018.03.025

Boyle, E. A., & Keigwin, L. D. (1985). Comparison of Atlantic and Pacific paleochemical records for the last 215,000 years: Changes in deep ocean circulation and chemical inventories. *Earth and Planetary Science Letters*, *76*(1-2), 135-150. https://doi.org/10.1016/0012-821X(85)90154-2

Broecker, W. S., & Peng, T.-H. (1982). Tracers in the sea. Palisades, New York: Eldigo.

Brown, S. J., & Elderfield, H. (1996). Variations in Mg/Ca and Sr/Ca ratios of planktonic foraminifera caused by postdepositional dissolution: Evidence of shallow Mg-dependent dissolution. *Paleoceanography*, *11*(5), 543-551. https://doi.org/10.1029/96PA01491

Burls, N. J., Bradshaw, C. D., De Boer, A. M., Herold, N., Huber, M., Pound, M., ... & Zhang, Z. (2021). Simulating Miocene warmth: insights from an opportunistic Multi-Model ensemble (MioMIP1). *Paleoceanography and Paleoclimatology*, e2020PA004054. https://doi.org/10.1029/2020PA004054

Cane, M. A., & Molnar, P. (2001). Closing of the Indonesian Seaway as the missing link between Pliocene East African aridi¢-cation and the Pacific. *Nature*, *6834*, 157-161. https://doi.org/10.1038/35075500

Carrapa, B., Clementz, M., & Feng, R. (2019). Ecological and hydroclimate responses to strengthening of the Hadley circulation in South America during the Late Miocene cooling. *Proceedings of the National Academy of Sciences*, *116*(20), 9747-9752. https://doi.org/10.1073/pnas.1810721116

Cerling, T. E., Harris, J. M., MacFadden, B. J., Leakey, M. G., Quade, J., Eisenmann, V., & Ehleringer, J. R. (1997). Global vegetation change through the Miocene/Pliocene boundary. *Nature*, *389*(6647), 153-158. https://doi.org/10.1038/38229

Clemens, S. C., Kuhnt, W., LeVay, L. J., Anand, P., Ando, T., Bartol, M., ... & Hathorne, E. C. (2016). Site U1443. In *Proceedings of the International Ocean Discovery Program* (Vol. 353). doi:10.14379/iodp.proc.353.102.2016

Clement, A. C., Hall, A., & Broccoli, A. J. (2004). The importance of precessional signals in the tropical climate. *Climate Dynamics*, *22*(4), 327-341. https://doi.org/10.1007/s00382-003-0375-8

Coggon, R. M., Teagle, D. A., Smith-Duque, C. E., Alt, J. C., & Cooper, M. J. (2010). Reconstructing past seawater Mg/Ca and Sr/Ca from mid-ocean ridge flank calcium carbonate veins. *Science*, *327*(5969), 1114-1117. DOI: 10.1126/science.1182252

Conte, M. H., Sicre, M. A., Rühlemann, C., Weber, J. C., Schulte, S., Schulz-Bull, D., & Blanz, T. (2006). Global temperature calibration of the alkenone unsaturation index (UK′ 37) in surface waters and comparison with surface sediments. *Geochemistry, Geophysics, Geosystems*, *7*(2). https://doi.org/10.1029/2005GC001054

Conte, M. H., Thompson, A., Lesley, D., & Harris, R. P. (1998). Genetic and physiological influences on the alkenone/alkenoate versus growth temperature relationship in Emiliania huxleyi and Gephyrocapsa oceanica. *Geochimica et Cosmochimica Acta*, *62*(1), 51-68. https://doi.org/10.1016/S0016-7037(97)00327-X

Dekens, P., D. Lea, D. Pak, and H. Spero (2002). Core top calibration of Mg/Ca in tropical foraminifera: Refining paleotemperature estimation, Geochem. Geophys. Geosyst., 3(4), 1022. https://doi.org/10.1029/2001GC000200

966 Delaney, M. L., Bé, A. W., & Boyle, E. A. (1985). Li, Sr, Mg, and Na in foraminiferal calcite
967 shells from laboratory culture, sediment traps, and sediment cores. *Geochimica et Cosmochimica*
968 *Acta*, *49*(6), 1327-1341. https://doi.org/10.1016/0016-7037(85)90284-4
969
970 Demicco, R. V., Lowenstein, T. K., Hardie, L. A., & Spencer, R. J. (2005). Model of seawater
971 composition for the Phanerozoic. *Geology*, *33*(11), 877-880. https://doi.org/10.1130/G21945.1
972
973 De Nooijer, L. J., Van Dijk, I., Toyofuku, T., & Reichart, G. J. (2017). The impacts of seawater
974 Mg/Ca and temperature on element incorporation in benthic foraminiferal calcite. *Geochemistry,*
975 *Geophysics, Geosystems*, *18*(10), 3617-3630.
976 https://doi.org/10.1002/2017GC007183
977
978 Dickson, J. A. D. (2002). Fossil echinoderms as monitor of the Mg/Ca ratio of Phanerozoic
979 oceans. *Science*, *298*(5596), 1222-1224. DOI: 10.1126/science.1075882
980
981 Dowsett, H. J., Foley, K. M., Stoll, D. K., Chandler, M. A., Sohl, L. E., Bentsen, M., ... & Zhang,
982 Z. (2013). Sea surface temperature of the mid-Piacenzian ocean: a data-model
983 comparison. *Scientific reports*, *3*(1), 1-8. https://doi.org/10.1038/srep02013
984
985 Drury, A. J., Lee, G. P., Gray, W. R., Lyle, M., Westerhold, T., Shevenell, A. E., & John, C. M.
986 (2018). Deciphering the state of the late Miocene to early Pliocene equatorial
987 Pacific. *Paleoceanography and Paleoclimatology*, *33*(3), 246-263.
988 https://doi.org/10.1002/2017PA003245
989
990 Drury, A. J., Liebrand, D., Westerhold, T., Beddow, H. M., Hodell, D. A., Rohlfs, N., ... &
991 Lourens, L. J. (2021). Climate, cryosphere and carbon cycle controls on Southeast Atlantic
992 orbital-scale carbonate deposition since the Oligocene (30–0 Ma). *Climate of the Past*, *17*(5),
993 2091-2117. https://doi.org/10.5194/cp-17-2091-2021
994

995 Drury, A. J., Westerhold, T., Frederichs, T., Tian, J., Wilkens, R., Channell, J. E., ... & Röhl, U.
996 (2017). Late Miocene climate and time scale reconciliation: Accurate orbital calibration from a
997 deep-sea perspective. *Earth and Planetary Science Letters*, *475*, 254-266.
998 https://doi.org/10.1016/j.epsl.2017.07.038
999
1000 Edgar, K. M., Anagnostou, E., Pearson, P. N., & Foster, G. L. (2015). Assessing the impact of
1001 diagenesis on δ11B, δ13C, δ18O, Sr/Ca and B/Ca values in fossil planktic foraminiferal calcite.
1002 *Geochimica et Cosmochimica Acta*, *166*, 189-209. https://doi.org/10.1016/j.gca.2015.06.018
1003
1004 Elderfield, H., Vautravers, M., & Cooper, M. (2002). The relationship between shell size and
1005 Mg/Ca, Sr/Ca, $\delta^{18}O$, and $\delta^{13}C$ of species of planktonic foraminifera. *Geochemistry, Geophysics,*
1006 *Geosystems*, *3*(8), 1-13. https://doi.org/10.1029/2001GC000194
1007
1008 Evans, D., Brierley, C., Raymo, M. E., Erez, J., & Müller, W. (2016). Planktic foraminifera shell
1009 chemistry response to seawater chemistry: Pliocene–Pleistocene seawater Mg/Ca, temperature
1010 and sea level change. *Earth and Planetary Science Letters*, *438*, 139-148.
1011 https://doi.org/10.1016/j.epsl.2016.01.013
1012
1013 Evans, D., & Müller, W. (2012). Deep time foraminifera Mg/Ca paleothermometry: Nonlinear
1014 correction for secular change in seawater Mg/Ca. *Paleoceanography*, *27*(4).
1015 https://doi.org/10.1029/2012PA002315
1016
1017 Fantle, M. S., & DePaolo, D. J. (2006). Sr isotopes and pore fluid chemistry in carbonate
1018 sediment of the Ontong Java Plateau: Calcite recrystallization rates and evidence for a rapid rise
1019 in seawater Mg over the last 10 million years. *Geochimica et Cosmochimica Acta*, *70*(15), 3883-
1020 3904. https://doi.org/10.1016/j.gca.2006.06.009
1021
1022 Farkaš, J., Böhm, F., Wallmann, K., Blenkinsop, J., Eisenhauer, A., Van Geldern, R., ... &
1023 Veizer, J. (2007). Calcium isotope record of Phanerozoic oceans: Implications for chemical
1024 evolution of seawater and its causative mechanisms. *Geochimica et Cosmochimica Acta*, *71*(21),
1025 5117-5134. https://doi.org/10.1016/j.gca.2007.09.004

Fichefet, T., & Maqueda, M. M. (1997). Sensitivity of a global sea ice model to the treatment of ice thermodynamics and dynamics. *Journal of Geophysical Research: Oceans*, *102*(C6), 12609-12646. https://doi.org/10.1029/97JC00480

Flower, B. P., & Kennett, J. P. (1994). The middle Miocene climatic transition: East Antarctic ice sheet development, deep ocean circulation and global carbon cycling. *Palaeogeography, palaeoclimatology, palaeoecology*, *108*(3-4), 537-555. https://doi.org/10.1016/0031-0182(94)90251-8

Friedrich, O., Schiebel, R., Wilson, P. A., Weldeab, S., Beer, C. J., Cooper, M. J., & Fiebig, J. (2012). Influence of test size, water depth, and ecology on Mg/Ca, Sr/Ca, $\delta^{18}O$ and $\delta^{13}C$ in nine modern species of planktic foraminifers. *Earth and Planetary Science Letters*, *319*, 133-145. https://doi.org/10.1016/j.epsl.2011.12.002

Gallagher, S. J., Wallace, M. W., Li, C. L., Kinna, B., Bye, J. T., Akimoto, K., & Torii, M. (2009). Neogene history of the West Pacific warm pool, Kuroshio and Leeuwin currents. *Paleoceanography*, *24*(1). https://doi.org/10.1029/2008PA001660

Goni, M. A., Hartz, D. M., Thunell, R. C., & Tappa, E. (2001). Oceanographic considerations for the application of the alkenone-based paleotemperature U37K′ index in the Gulf of California. *Geochimica et Cosmochimica Acta*, *65*(4), 545-557. https://doi.org/10.1016/S0016-7037(00)00559-7

Gordon, A. L. (2005). Oceanography of the Indonesian seas and their throughflow. *Oceanography*, *18*(4), 14-27.

Gordon, A. L., & Fine, R. A. (1996). Pathways of water between the Pacific and Indian oceans in the Indonesian seas. *Nature*, *379*(6561), 146-149. https://doi.org/10.1038/379146a0

Gothmann, A. M., Stolarski, J., Adkins, J. F., Schoene, B., Dennis, K. J., Schrag, D. P., ... & Bender, M. L. (2015). Fossil corals as an archive of secular variations in seawater chemistry since the Mesozoic. *Geochimica et Cosmochimica Acta*, *160*, 188-208. https://doi.org/10.1016/j.gca.2015.03.018

Gouhier, T. C., Grinsted, A., and Simko, V. (2016). Package 'biwavelet' [code].

Gray, W. R., & Evans, D. (2019). Nonthermal influences on Mg/Ca in planktonic foraminifera: A review of culture studies and application to the last glacial maximum. *Paleoceanography and Paleoclimatology*, *34*(3), 306-315. https://doi.org/10.1029/2018PA003517

Greaves, M. J., Barker, S., Daunt, C., & Elderfield, H. (2005). Accuracy, standardisation and interlaboratory calibration standards for foraminiferal Mg/Ca thermometry [Technical Brief]. *G3 Geochemistry Geophysics Geosystems*, *6*(2). https://doi.org/10.1029/2004GC000790

Grimalt, J. O., Calvo, E., & Pelejero, C. (2001). Sea surface paleotemperature errors in UK'_{37} estimation due to alkenone measurements near the limit of detection. *Paleoceanography*, *16*(2), 226-232. https://doi.org/10.1029/1999PA000440

Grinsted, A., Moore, J. C., and Jevrejeva, S. (2004). Application of the cross wavelet transform and wavelet coherence to geophysical time series. https://doi.org/10.5194/npg-11-561-2004

Gupta, A. K., Yuvaraja, A., Prakasam, M., Clemens, S. C., & Velu, A. (2015). Evolution of the South Asian monsoon wind system since the late Middle Miocene. *Palaeogeography, Palaeoclimatology, Palaeoecology*, *438*, 160-167. https://doi.org/10.1016/j.palaeo.2015.08.006

Gupta, S. M., Fernandes, A. A., & Mohan, R. (1996). Tropical sea surface temperatures and the Earth's orbital eccentricity cycles. *Geophysical Research Letters*, *23*(22), 3159-3162. https://doi.org/10.1029/96GL02923

1085 Hall, R. (2002). Cenozoic geological and plate tectonic evolution of SE Asia and the SW Pacific:
1086 computer-based reconstructions, model and animations. *Journal of Asian Earth Sciences*, *20*(4),
1087 353-431. https://doi.org/10.1016/S1367-9120(01)00069-4
1088
1089 Hall, R. (2009). Southeast Asia's changing palaeogeography. *Blumea-Biodiversity, Evolution and*
1090 *Biogeography of Plants*, *54*(1-2), 148-161. https://doi.org/10.3767/000651909X475941
1091
1092 Hall, R., Audley-Charles, M. G., Banner, F. T., Hidayat, S., & Tobing, S. L. (1988). Late
1093 Palaeogene–Quaternary geology of Halmahera, Eastern Indonesia: initiation of a volcanic island
1094 arc. *Journal of the Geological Society*, *145*(4), 577-590. https://doi.org/10.1144/gsjgs.145.4.0577
1095
1096 Hall, R., Gower, D. J., Johnson, K. G., Richardson, J. E., Rosen, B. R., Rüber, L., & Williams, S.
1097 T. (2012). Sundaland and Wallacea: geology, plate tectonics and palaeogeography. *Biotic*
1098 *evolution and environmental change in Southeast Asia*, *32*, 78.
1099
1100 Haywood, A. M., Tindall, J. C., Dowsett, H. J., Dolan, A. M., Foley, K. M., Hunter, S. J., ... &
1101 Lunt, D. J. (2020). A return to large-scale features of Pliocene climate: the Pliocene Model
1102 Intercomparison Project Phase 2. *Climate of the Past*. https://doi.org/10.5194/cp-2019-145
1103
1104 Hemleben, C., Spindler, M., & Anderson, O. R. (2012). *Modern planktonic foraminifera*.
1105 Springer Science & Business Media.
1106
1107 Herbert, T. D., Lawrence, K. T., Tzanova, A., Peterson, L. C., Caballero-Gill, R., & Kelly, C. S.
1108 (2016). Late Miocene global cooling and the rise of modern ecosystems. *Nature*
1109 *Geoscience*, *9*(11), 843-847. https://doi.org/10.1038/ngeo2813
1110
1111 Herbert, T. D., Peterson, L. C., Lawrence, K. T., & Liu, Z. (2010). Tropical ocean temperatures
1112 over the past 3.5 million years. *science*, *328*(5985), 1530-1534. DOI: 10.1126/science.1185435
1113

1114 Higgins, J. A., & Schrag, D. P. (2012). Records of Neogene seawater chemistry and diagenesis
1115 in deep-sea carbonate sediments and pore fluids. *Earth and Planetary Science Letters*, *357*, 386-
1116 396. https://doi.org/10.1016/j.epsl.2012.08.030
1117
1118 Higgins, J. A., & Schrag, D. P. (2015). The Mg isotopic composition of Cenozoic seawater–
1119 evidence for a link between Mg-clays, seawater Mg/Ca, and climate. *Earth and Planetary*
1120 *Science Letters*, *416*, 73-81. https://doi.org/10.1016/j.epsl.2015.01.003
1121
1122 Hilgen, F., Zeeden, C., & Laskar, J. (2020). Paleoclimate records reveal elusive~ 200-kyr
1123 eccentricity cycle for the first time. *Global and Planetary Change*, *194*, 103296.
1124 https://doi.org/10.1016/j.gloplacha.2020.103296
1125
1126 Ho, S. L., & Laepple, T. (2015). Glacial cooling as inferred from marine temperature proxies
1127 TEXH86 and UK′ 37. *Earth and Planetary Science Letters*, *409*, 15-22.
1128 https://doi.org/10.1016/j.epsl.2014.10.033
1129
1130 Ho, S. L., & Laepple, T. (2016). Flat meridional temperature gradient in the early Eocene in the
1131 subsurface rather than surface ocean. *Nature Geoscience*, *9*(8), 606-610.
1132 https://doi.org/10.1038/ngeo2763
1133
1134 Hodell, D. A., Curtis, J. H., Sierro, F. J., & Raymo, M. E. (2001). Correlation of late Miocene to
1135 early Pliocene sequences between the Mediterranean and North
1136 Atlantic. *Paleoceanography*, *16*(2), 164-178. https://doi.org/10.1029/1999PA000487
1137
1138 Hodell, D. A., & Vayavananda, A. (1993). Middle Miocene paleoceanography of the western
1139 equatorial Pacific (DSDP site 289) and the evolution ofGloborotalia (Fohsella). *Marine*
1140 *Micropaleontology*, *22*(4), 279-310. https://doi.org/10.1016/0377-8398(93)90019-T
1141
1142 Holbourn, A. E., Kuhnt, W., Clemens, S. C., Kochhann, K. G., Jöhnck, J., Lübbers, J., &
1143 Andersen, N. (2018). Late Miocene climate cooling and intensification of southeast Asian winter
1144 monsoon. *Nature Communications*, *9*(1), 1-13. https://doi.org/10.1038/s41467-018-03950-1

Holbourn, A., Kuhnt, W., Lyle, M., Schneider, L., Romero, O., & Andersen, N. (2014). Middle Miocene climate cooling linked to intensification of eastern equatorial Pacific upwelling. *Geology*, *42*(1), 19-22. https://doi.org/10.1130/G34890.1

Hollstein, M., Mohtadi, M., Rosenthal, Y., Moffa Sanchez, P., Oppo, D., Martínez Méndez, G., ... & Hebbeln, D. (2017). Stable oxygen isotopes and Mg/Ca in planktic foraminifera from modern surface sediments of the Western Pacific Warm Pool: Implications for thermocline reconstructions. *Paleoceanography*, *32*(11), 1174-1194. https://doi.org/10.1002/2017PA003122

Horita, J., H. Zimmermann, and H. Holland (2002). Chemical evolution of seawater during the Phanerozoic: Implications from the record of marine evaporites, Geochim. Cosmochim. Acta, 66(21), 3733–3756. https://doi.org/10.1016/S0016-7037(01)00884-5

Hourdin, F., Foujols, M. A., Codron, F., Guemas, V., Dufresne, J. L., Bony, S., ... & Bopp, L. (2013). Impact of the LMDZ atmospheric grid configuration on the climate and sensitivity of the IPSL-CM5A coupled model. *Climate Dynamics*, *40*(9-10), 2167-2192. DOI 10.1007/s00382-012-1411-3

Huang, Y., Clemens, S. C., Liu, W., Wang, Y., & Prell, W. L. (2007).Large-scale hydrological change drove the late Miocene C4 plant expansion in the Himalayan foreland and Arabian Peninsula. *Geology*, *35*(6), 531-534. https://doi.org/10.1130/G23666A.1

Jensen, T. G. (2001). Arabian Sea and Bay of Bengal exchange of salt and tracers in an ocean model. *Geophysical Research Letters*, *28*(20), 3967-3970. https://doi.org/10.1029/2001GL013422

Jensen, T. G. (2003). Cross-equatorial pathways of salt and tracers from the northern Indian Ocean: Modelling results. *Deep Sea Research Part II: Topical Studies in Oceanography*, *50*(12-13), 2111-2127. https://doi.org/10.1016/S0967-0645(03)00048-1

1176 Jöhnck, J., Kuhnt, W., Holbourn, A., & Andersen, N. (2020). Variability of the Indian Monsoon
1177 in the Andaman Sea Across the Miocene-Pliocene Transition. *Paleoceanography and*
1178 *Paleoclimatology*, *35*(9), e2020PA003923. https://doi.org/10.1029/2020PA003923
1179
1180 John, K. E. S., & Krissek, L. A. (2002). The late Miocene to Pleistocene ice-rafting history of
1181 southeast Greenland. *Boreas*, *31*(1), 28-35. https://doi.org/10.1111/j.1502-3885.2002.tb01053.x
1182
1183 Jonkers, L., Brummer, G. J. A., Peeters, F. J., van Aken, H. M., & De Jong, M. F. (2010).
1184 Seasonal stratification, shell flux, and oxygen isotope dynamics of left-coiling N. pachyderma
1185 and T. quinqueloba in the western subpolar North Atlantic. *Paleoceanography*, *25*(2).
1186 https://doi.org/10.1029/2009PA001849
1187
1188 Jonkers, L., Van Heuven, S., Zahn, R., & Peeters, F. J. (2013). Seasonal patterns of shell flux,
1189 δ18O and δ13C of small and large N. pachyderma (s) and G. bulloides in the subpolar North
1190 Atlantic. *Paleoceanography*, *28*(1), 164-174. https://doi.org/10.1002/palo.20018
1191
1192 Keerthi, M. G., Lengaigne, M., Vialard, J., de Boyer Montégut, C., & Muraleedharan, P. M.
1193 (2013). Interannual variability of the Tropical Indian Ocean mixed layer depth. *Climate*
1194 *dynamics*, *40*(3), 743-759. https://doi.org/10.1007/s00382-012-1295-2
1195
1196 Keigwin Jr, L. D. (1979). Late Cenozoic stable isotope stratigraphy and paleoceanography of
1197 DSDP sites from the east equatorial and central North Pacific Ocean. *Earth and Planetary*
1198 *Science Letters*, *45*(2), 361-382. https://doi.org/10.1016/0012-821X(79)90137-7
1199
1200 Keigwin, L. D., & Shackleton, N. J. (1980). Uppermost Miocene carbon isotope stratigraphy of a
1201 piston core in the equatorial Pacific. *Nature*, *284*(5757), 613-614.
1202 https://doi.org/10.1038/284613a0
1203
1204 Kennett, J.P., Keller, G., Srinivasan, M.S., (1985). Miocene planktonic foraminiferal
1205 biogeography and pale-oceanographic development of the Indo-Pacific region. *The Miocene*

1206 *Ocean: Paleoceanography and biogeography: Boulder, Colorado Geologic Society of America*
1207 *Memoir*, 197-236. https://doi.org/10.1130/MEM163-p197
1208
1209 Knorr, G., Butzin, M., Micheels, A., & Lohmann, G. (2011). A warm Miocene climate at low
1210 atmospheric CO2 levels. *Geophysical Research Letters*, *38*(20).
1211 https://doi.org/10.1029/2011GL048873
1212
1213 Kodama, K. P., & Hinnov, L. A. (2014). *Rock magnetic cyclostratigraphy* (Vol. 5). John Wiley
1214 & Sons. DOI:10.1002/9781118561294
1215
1216 Krebs, U., Park, W., & Schneider, B. (2011). Pliocene aridification of Australia caused by
1217 tectonically induced weakening of the Indonesian throughflow. *Palaeogeography,*
1218 *Palaeoclimatology, Palaeoecology*, *309*(1-2), 111-117.
1219 https://doi.org/10.1016/j.palaeo.2011.06.002
1220
1221 Krinner, G., Ciais, P., Viovy, N., & Friedlingstein, P. (2005). A simple parameterization of
1222 nitrogen limitation on primary productivity for global vegetation models. *Biogeosciences*
1223 *Discussions*, *2*(4), 1243-1282. https://doi.org/10.5194/bgd-2-1243-2005
1224
1225 Krissek, L. A. (1995). Late Cenozoic ice-rafting records from Leg 145 sites in the North Pacific:
1226 Late Miocene onset, late Pliocene intensification, and Plio-Pleistocene events. In *Proc. Ocean*
1227 *Drill. Program Sci. Results* (Vol. 145, pp. 179-194).
1228
1229 Kuhnt, W., Holbourn, A., Hall, R., Zuvela, M., & Käse, R. (2004). Neogene history of the
1230 Indonesian throughflow. *Continent-Ocean Interactions within East Asian Marginal Seas.*
1231 *Geophysical Monograph*, *149*, 299-320. https://doi.org/10.1029/149GM16
1232
1233 Kürschner, W. M., van der Burgh, J., Visscher, H., & Dilcher, D. L. (1996). Oak leaves as
1234 biosensors of late Neogene and early Pleistocene paleoatmospheric CO2 concentrations. *Marine*
1235 *Micropaleontology*, *27*(1-4), 299-312. https://doi.org/10.1016/0377-8398(95)00067-4
1236

1237 LaRiviere, J. P., Ravelo, A. C., Crimmins, A., Dekens, P. S., Ford, H. L., Lyle, M., & Wara, M.
1238 W. (2012). Late Miocene decoupling of oceanic warmth and atmospheric carbon dioxide
1239 forcing. *Nature*, *486*(7401), 97-100. https://doi.org/10.1038/nature11200
1240
1241 Larsen, H. C., Saunders, A. D., Clift, P. D., Beget, J., Wei, W., & Spezzaferri, S. (1994). Seven
1242 million years of glaciation in Greenland. *Science*, *264*(5161), 952-955. DOI:
1243 10.1126/science.264.5161.952
1244
1245 Lawrence, K. T., Liu, Z., & Herbert, T. D. (2006). Evolution of the eastern tropical Pacific
1246 through Plio-Pleistocene glaciation. *Science*, *312*(5770), 79-83.
1247 https://doi.org/10.1126/science.1120395
1248
1249 Lea, D. W. (2004). The 100 000-yr cycle in tropical SST, greenhouse forcing, and climate
1250 sensitivity. *Journal of Climate*, *17*(11), 2170-2179. https://doi.org/10.1175/1520-
1251 0442(2004)017<2170:TYCITS>2.0.CO;2
1252
1253 Lea, D. W., Mashiotta, T. A., & Spero, H. J. (1999). Controls on magnesium and strontium
1254 uptake in planktonic foraminifera determined by live culturing. *Geochimica et Cosmochimica*
1255 *Acta*, *63*(16), 2369-2379. https://doi.org/10.1016/S0016-7037(99)00197-0
1256
1257 Lea, D. W., Pak, D. K., Belanger, C. L., Spero, H. J., Hall, M. A., & Shackleton, N. J. (2006).
1258 Paleoclimate history of Galapagos surface waters over the last 135,000 yr. *Quaternary Science*
1259 *Reviews*, *25*(11-12), 1152-1167. https://doi.org/10.1016/j.quascirev.2005.11.010
1260
1261 Lear, C. H., Elderfield, H., & Wilson, P. A. (2000). Cenozoic deep-sea temperatures and global
1262 ice volumes from Mg/Ca in benthic foraminiferal calcite. *science*, *287*(5451), 269-272. DOI:
1263 10.1126/science.287.5451.269
1264
1265 Leduc, G., Garidel-Thoron, T. D., Kaiser, J., Bolton, C., & Contoux, C. (2017). Databases for
1266 sea surface paleotemperature based on geochemical proxies from marine sediments: implications

1267 for model-data comparisons. *Quaternaire. Revue de l'Association française pour l'étude du*
1268 *Quaternaire*, *28*(2), 201-216. https://doi.org/10.4000/quaternaire.8034
1269
1270 Levy, R. H., Meyers, S. R., Naish, T. R., Golledge, N. R., McKay, R. M., Crampton, J. S., ... &
1271 Kulhanek, D. K. (2019). Antarctic ice-sheet sensitivity to obliquity forcing enhanced through
1272 ocean connections. *Nature Geoscience*, *12*(2), 132-137. https://doi.org/10.1038/s41561-018-
1273 0284-4
1274
1275 Li, D., Zhao, M., & Tian, J. (2017). Low-high latitude interaction forcing on the evolution of the
1276 400 kyr cycle in East Asian winter monsoon records during the last 2.8 Myr. *Quaternary Science*
1277 *Reviews*, *172*, 72-82. https://doi.org/10.1016/j.quascirev.2017.08.005
1278
1279 Li, L., Li, Q., Tian, J., Wang, P., Wang, H., & Liu, Z. (2011). A 4-Ma record of thermal
1280 evolution in the tropical western Pacific and its implications on climate change. *Earth and*
1281 *Planetary Science Letters*, *309*(1-2), 10-20. https://doi.org/10.1016/j.epsl.2011.04.016
1282
1283 Li, M., Hinnov, L., & Kump, L. (2019). Acycle: Time-series analysis software for paleoclimate
1284 research and education. *Computers & geosciences*, *127*, 12-22.
1285 https://doi.org/10.1016/j.cageo.2019.02.011
1286
1287 Li, Q., Li, B., Zhong, G., McGowran, B., Zhou, Z., Wang, J., & Wang, P. (2006). Late Miocene
1288 development of the western Pacific warm pool: Planktonic foraminifer and oxygen isotopic
1289 evidence. *Palaeogeography, Palaeoclimatology, Palaeoecology*, *237*(2-4), 465-482.
1290 https://doi.org/10.1016/j.palaeo.2005.12.019
1291
1292 Lipp, J. S., & Hinrichs, K. U. (2009). Structural diversity and fate of intact polar lipids in marine
1293 sediments. *Geochimica et Cosmochimica Acta*, *73*(22), 6816-6833.
1294 https://doi.org/10.1016/j.gca.2009.08.003
1295

1296 Liu, J., Tian, J., Liu, Z., Herbert, T. D., Fedorov, A. V., & Lyle, M. (2019). Eastern equatorial
1297 Pacific cold tongue evolution since the late Miocene linked to extratropical climate. *Science*
1298 *advances*, *5*(4), eaau6060. DOI: 10.1126/sciadv.aau6060
1299
1300 Liu, X., Huber, M., Foster, G. L., Leckie, R. M., & Zhang, Y. G. (2020, May). Persistent high
1301 latitude amplification over the past 10 million years. In *EGU General Assembly Conference*
1302 *Abstracts* (p. 597).
1303
1304 Liu, Z., Cleaveland, L. C., & Herbert, T. D. (2008). Early onset and origin of 100-kyr cycles in
1305 Pleistocene tropical SST records. *Earth and Planetary Science Letters*, *265*(3-4), 703-715.
1306 https://doi.org/10.1016/j.epsl.2007.11.016
1307
1308 Liu, Z., & Herbert, T. D. (2004). High-latitude influence on the eastern equatorial Pacific climate
1309 in the early Pleistocene epoch. *Nature*, *427*(6976), 720-723. https://doi.org/10.1038/nature02338
1310
1311 Locarnini, M., Mishonov, A. V., Baranova, O. K., Boyer, T. P., Zweng, M. M., Garcia, H. E.,
1312 Reagan, J.R., Seidov, D., Weathers, K., Paver, C. R., and Smolyar, I. (2018). *World Ocean Atlas*
1313 *2018, Volume 1: Temperature*. A. Mishonov Technical Ed.; NOAA Atlas NESDIS 81, 52pp.
1314 https://archimer.ifremer.fr/doc/00651/76338/
1315
1316 Locarnini, R., Mishonov, A. V., Antonov, J. I., Boyer, T. P., Garcia, H.E., Baranova, O.K.,
1317 Zweng, M. M., Paver, C. R., Reagan, J. R., Johnson, D. R., Hamilton, M., and D. Seidov, D.
1318 (2013). *World Ocean Atlas 2013, Volume 1: Temperature.* S. Levitus, Ed., A. Mishonov
1319 Technical Ed.; NOAA Atlas NESDIS 73, 40 pp.
1320
1321 Lowenstein, T., M. Timofeeff, S. Brennan, L. Hardie, and R. Demicco (2001). Oscillations in
1322 Phanerozoic seawater chemistry: Evidence from fluid inclusions, Science, 294, 1086–1088. DOI:
1323 10.1126/science.1064280
1324

Lukas, R., & Webster, P. (1989). TOGA-COARE: a coupled ocean-atmospheric response experiment for the warm pool regions of the western Pacific. *Scientific plan compiled by R Lukas and P Webster*.

Lüthi, D., Le Floch, M., Bereiter, B., Blunier, T., Barnola, J. M., Siegenthaler, U., ... & Stocker, T. F. (2008). High-resolution carbon dioxide concentration record 650,000–800,000 years before present. *nature*, *453*(7193), 379-382. https://doi.org/10.1038/nature06949

Madec, G. & Nemo, T. NEMO ocean engine. *Note du Pôle de modélisation de l'Institut Pierre Simon Laplace* 27 (2015).

Madec, G. NEMO reference manual, ocean dynamics component: NEMO-OPA. *Preliminary version. Note du Pole de modélisation, Institut Pierre-Simon Laplace (IPSL), France*, 1288-1161 (2008).

Mashiotta, T. A., Lea, D. W., & Spero, H. J. (1999). Glacial–interglacial changes in Subantarctic sea surface temperature and δ18O-water using foraminiferal Mg. *Earth and Planetary Science Letters*, *170*(4), 417-432. https://doi.org/10.1016/S0012-821X(99)00116-8

Mathien-Blard, E., & Bassinot, F. (2009). Salinity bias on the foraminifera Mg/Ca thermometry: Correction procedure and implications for past ocean hydrographic reconstructions. *Geochemistry, Geophysics, Geosystems*, *10*(12). https://doi.org/10.1029/2008GC002353

Medina-Elizalde, M., Lea, D. W., & Fantle, M. S. (2008). Implications of seawater Mg/Ca variability for Plio-Pleistocene tropical climate reconstruction. *Earth and Planetary Science Letters*, *269*(3-4), 585-595. https://doi.org/10.1016/j.epsl.2010.08.016

Mejia, L. M., Bernasconi, S. M., Fernandez, A., Zhang, H., Guitian, J., Perez-Huerta, A., & Stoll, H. M. (2020, December). Coccolith clumped isotopes suggest a more modest Miocene North Atlantic polar amplification. In *AGU Fall Meeting Abstracts*(Vol. 2020, pp. PP001-0002).

Mejía, L. M., Méndez-Vicente, A., Abrevaya, L., Lawrence, K. T., Ladlow, C., Bolton, C., ... & Stoll, H. (2017). A diatom record of CO2 decline since the late Miocene. *Earth and Planetary Science Letters*, *479*, 18-33. https://doi.org/10.1016/j.epsl.2017.08.034

Miller, K. G., Browning, J. V., Schmelz, W. J., Kopp, R. E., Mountain, G. S., & Wright, J. D. (2020). Cenozoic sea-level and cryospheric evolution from deep-sea geochemical and continental margin records. *Science advances*, *6*(20), eaaz1346. DOI: 10.1126/sciadv.aaz1346

Mix, A. C. (2003). Chapter 12, Site 1241. In *Proc. Ocean Drill. Program Initial Rep* (Vol. 202, p. 101). DOI:10.2973/odp.proc.ir.202.112.2003

Molnar, P., & Cronin, T. W. (2015). Growth of the Maritime Continent and its possible contribution to recurring Ice Ages. *Paleoceanography*, *30*(3), 196-225. https://doi.org/10.1002/2014PA002752

Müller, P. J., Kirst, G., Ruhland, G., Von Storch, I., & Rosell-Melé, A. (1998). Calibration of the alkenone paleotemperature index U37K′ based on core-tops from the eastern South Atlantic and the global ocean (60° N-60° S). *Geochimica et Cosmochimica Acta*, *62*(10), 1757-1772. https://doi.org/10.1016/S0016-7037(98)00097-0

Nathan, S. A., & Leckie, R. M. (2009). Early history of the Western Pacific Warm Pool during the middle to late Miocene (~ 13.2–5.8 Ma): Role of sea-level change and implications for equatorial circulation. *Palaeogeography, Palaeoclimatology, Palaeoecology*, *274*(3-4), 140-159. https://doi.org/10.1016/j.palaeo.2009.01.007

O'Brien, C. L., Foster, G. L., Martínez-Botí, M. A., Abell, R., Rae, J. W., & Pancost, R. D. (2014). High sea surface temperatures in tropical warm pools during the Pliocene. *Nature Geoscience*, *7*(8), 606-611. https://doi.org/10.1038/ngeo2194

1386 Ohneiser, C., Florindo, F., Stocchi, P., Roberts, A. P., DeConto, R. M., & Pollard, D. (2015).
1387 Antarctic glacio-eustatic contributions to late Miocene Mediterranean desiccation and
1388 reflooding. *Nature communications*, *6*(1), 1-10. https://doi.org/10.1038/ncomms9765
1389
1390 Otto-Bliesner, B. L., Jahn, A., Feng, R., Brady, E. C., Hu, A., & Löfverström, M. (2017).
1391 Amplified North Atlantic warming in the late Pliocene by changes in Arctic
1392 gateways. *Geophysical Research Letters*, *44*(2), 957-964. https://doi.org/10.1002/2016GL071805
1393
1394 Pagani, M., Freeman, K. H., & Arthur, M. A. (1999). Late Miocene atmospheric CO2
1395 concentrations and the expansion of C4 grasses. *Science*, *285*(5429), 876-879. DOI:
1396 10.1126/science.285.5429.876
1397
1398 Pagani, M., Zachos, J. C., Freeman, K. H., Tipple, B., & Bohaty, S. (2005). Marked decline in
1399 atmospheric carbon dioxide concentrations during the Paleogene. *Science*, *309*(5734), 600-603.
1400 DOI: 10.1126/science.1110063
1401
1402 Past Interglacials Working Group of PAGES. (2016). Interglacials of the last 800,000
1403 years. *Reviews of Geophysics*, *54*(1), 162-219.
1404
1405 Pelejero, C., & Calvo, E. (2003). The upper end of the UK′ 37 temperature calibration
1406 revisited. *Geochemistry, Geophysics, Geosystems*, *4*(2). https://doi.org/10.1029/2002GC000431
1407
1408 Petit, J. R., Jouzel, J., Raynaud, D., Barkov, N. I., Barnola, J. M., Basile, I., ... & Stievenard, M.
1409 (1999). Climate and atmospheric history of the past 420,000 years from the Vostok ice core,
1410 Antarctica. *Nature*, *399*(6735), 429-436. https://doi.org/10.1038/20859
1411
1412 Poole, C. R., & Wade, B. S. (2019). Systematic taxonomy of the Trilobatus sacculifer plexus and
1413 descendant Globigerinoidesella fistulosa (planktonic foraminifera). *Journal of Systematic*
1414 *Palaeontology*, *17*(23), 1989-2030. https://doi.org/10.1080/14772019.2019.1578831
1415

1416 Pound, M. J., Haywood, A. M., Salzmann, U., & Riding, J. B. (2012). Global vegetation
1417 dynamics and latitudinal temperature gradients during the Mid to Late Miocene (15.97–5.33
1418 Ma). *Earth-Science Reviews*, *112*(1-2), 1-22. https://doi.org/10.1016/j.earscirev.2012.02.005
1419
1420 Prahl, F. G., Muehlhausen, L. A., & Zahnle, D. L. (1988). Further evaluation of long-chain
1421 alkenones as indicators of paleoceanographic conditions. *Geochimica et Cosmochimica*
1422 *Acta*, *52*(9), 2303-2310. https://doi.org/10.1016/0016-7037(88)90132-9
1423
1424 Rae, J. W., Zhang, Y. G., Liu, X., Foster, G. L., Stoll, H. M., & Whiteford, R. D. (2021).
1425 Atmospheric CO2 over the Past 66 Million Years from Marine Archives. *Annual Review of*
1426 *Earth and Planetary Sciences*, *49*. https://doi.org/10.1146/annurev-earth-082420-063026
1427
1428 Ramaswamy, V., & Gaye, B. (2006). Regional variations in the fluxes of foraminifera carbonate,
1429 coccolithophorid carbonate and biogenic opal in the northern Indian Ocean. *Deep Sea Research*
1430 *Part I: Oceanographic Research Papers*, *53*(2), 271-293.
1431 https://doi.org/10.1016/j.dsr.2005.11.003
1432
1433 Rao, R. R., & Sivakumar, R. (2003). Seasonal variability of sea surface salinity and salt budget
1434 of the mixed layer of the north Indian Ocean. *Journal of Geophysical Research:*
1435 *Oceans*, *108*(C1), 9-1. https://doi.org/10.1029/2001JC000907
1436
1437 Retallack, G. J. (2009). Greenhouse crises of the past 300 million years. *Geological Society of*
1438 *America Bulletin*, *121*(9-10), 1441-1455. https://doi.org/10.1130/B26341.1
1439
1440 Reuss, A. V. (1850). Neues Foraminiferen aus den schicten des Osterreichischen
1441 Tertiarbeckens. *Denkschriften der Akademie des Wissenschaften Wein*, *1*, 365-390.
1442
1443 Richey, J. N., & Tierney, J. E. (2016). GDGT and alkenone flux in the northern Gulf of Mexico:
1444 Implications for the TEX86 and UK'37 paleothermometers. *Paleoceanography*, *31*(12), 1547-
1445 1561. https://doi.org/10.1002/2016PA003032
1446

1447 Rixen, T., Gaye, B., Emeis, K. C., & Ramaswamy, V. (2019). The ballast effect of lithogenic
1448 matter and its influences on the carbon fluxes in the Indian Ocean. *Biogeosciences*, *16*(2), 485-
1449 503. https://doi.org/10.5194/bg-16-485-2019
1450
1451 Rommerskirchen, F., Condon, T., Mollenhauer, G., Dupont, L., & Schefuss, E. (2011). Miocene
1452 to Pliocene development of surface and subsurface temperatures in the Benguela Current
1453 system. *Paleoceanography*, *26*(3). https://doi.org/10.1029/2010PA002074
1454
1455 Rosenthal, Y., & Lohmann, G. P. (2002). Accurate estimation of sea surface temperatures using
1456 dissolution-corrected calibrations for Mg/Ca paleothermometry. *Paleoceanography*, *17*(3), 16-1.
1457 https://doi.org/10.1029/2001PA000749
1458
1459 Rosenthal, Y., Lohmann, G. P., Lohmann, K. C., & Sherrell, R. M. (2000). Incorporation and
1460 preservation of Mg in Globigerinoides sacculifer: Implications for reconstructing the temperature
1461 and 18O/16O of seawater. *Paleoceanography*, *15*(1), 135-145.
1462 https://doi.org/10.1029/1999PA000415
1463
1464 Rosenthal, Y., Perron-Cashman, S., Lear, C. H., Bard, E., Barker, S., Billups, K., ... & Elderfield,
1465 H. (2004). Interlaboratory comparison study of Mg/Ca and Sr/Ca measurements in planktonic
1466 foraminifera for paleoceanographic research.*Geochemistry, Geophysics, Geosystems*, *5*(4).
1467 https://doi.org/10.1029/2003GC000650
1468
1469 Rousselle, G., Beltran, C., Sicre, M. A., Raffi, I., & De Rafelis, M. (2013). Changes in sea-
1470 surface conditions in the Equatorial Pacific during the middle Miocene–Pliocene as inferred from
1471 coccolith geochemistry. *Earth and planetary science letters*, *361*, 412-421.
1472 https://doi.org/10.1016/j.epsl.2012.11.003
1473
1474 Sarr, A.-C., Y. Donnadieu, C. T. Bolton, J.-B. Ladant, A. Licht, F. Fluteau, M. Laugié, D. Tardif,
1475 and G. Dupont-Nivet (in review), Reconciling South Asian Monsoon Rainfall and Wind
1476 Histories, Nature Geoscience.
1477

1478 Schiebel, R., & Hemleben, C. (2017). *Planktic foraminifers in the modern ocean* (pp. 1-358).
1479 Berlin: Springer. DOI 10.1007/978-3-662-50297-6
1480
1481 Schott, F. A., Xie, S. P., & McCreary Jr, J. P. (2009). Indian Ocean circulation and climate
1482 variability. *Reviews of Geophysics*, *47*(1). https://doi.org/10.1029/2007RG000245
1483
1484 Scotese, C. R. (2016). Tutorial: PALEOMAP PaleoAtlas for GPlates and the PaleoData Plotter
1485 Program. http://www.earthbyte.org/paleomap-paleoatlas-for-gplates/
1486
1487 Seki, O., Schmidt, D. N., Schouten, S., Hopmans, E. C., Sinninghe Damsté, J. S., & Pancost, R.
1488 D. (2012). Paleoceanographic changes in the Eastern Equatorial Pacific over the last 10
1489 Myr. *Paleoceanography*, *27*(3). https://doi.org/10.1029/2011PA002158
1490
1491 Sepulchre, P., Caubel, A., Ladant, J. B., Bopp, L., Boucher, O., Braconnot, P., ... & Tardif, D.
1492 (2020). IPSL-CM5A2–an Earth system model designed for multi-millennial climate
1493 simulations. *Geoscientific Model Development*, *13*(7), 3011-3053. https://doi.org/10.5194/gmd-
1494 13-3011-2020
1495
1496 Sexton, P. F., Wilson, P. A., & Pearson, P. N. (2006). Microstructural and geochemical
1497 perspectives on planktic foraminiferal preservation:“Glassy” versus “Frosty”. *Geochemistry,*
1498 *Geophysics, Geosystems*, *7*(12). https://doi.org/10.1029/2006GC001291
1499
1500 Shackleton, N. J., Hall, M. A., & Pate, D. (1995). 15. Pliocene stable isotope stratigraphy of Site
1501 846. In *Proc. Ocean Drill. Program Sci. Results* (Vol. 138, pp. 337-355).
1502
1503 Shakun, J. D., Raymo, M. E., & Lea, D. W. (2016). An early Pleistocene Mg/Ca-δ18O record
1504 from the Gulf of Mexico: Evaluating ice sheet size and pacing in the 41-kyr
1505 world. *Paleoceanography*, *31*(7), 1011-1027. https://doi.org/10.1002/2016PA002956
1506
1507 Shetye, S. R., Gouveia, A. D., Shankar, D., Shenoi, S. S. C., Vinayachandran, P. N., Sundar, D.,
1508 ... & Nampoothiri, G. (1996). Hydrography and circulation in the western Bay of Bengal during

1509 the northeast monsoon. *Journal of Geophysical Research: Oceans*, *101*(C6), 14011-
1510 14025. https://doi.org/10.1029/95JC03307
1511
1512 Shipboard Scientific Party, (1989). Site 758. *In* Peirce, J., Weissel, J., et al., *Proc. ODP, Init.*
1513 *Repts.,* 121: College Station, TX (Ocean Drilling Program), 359–453.
1514
1515 Sonzogni, C., Bard, E., & Rostek, F. (1998). Tropical sea-surface temperatures during the last
1516 glacial period: A view based on alkenones in Indian Ocean sediments. *Quaternary Science*
1517 *Reviews*, *17*(12), 1185–1201. https://doi.org/10.1016/S0277-3791(97)00099-1
1518
1519 Sosdian, S. M., Greenop, R., Hain, M. P., Foster, G. L., Pearson, P. N., & Lear, C. H. (2018).
1520 Constraining the evolution of Neogene ocean carbonate chemistry using the boron isotope pH
1521 proxy. *Earth and Planetary Science Letters*, *498*, 362-376.
1522 https://doi.org/10.1016/j.epsl.2018.06.017
1523
1524 Sosdian, S. M., & Lear, C. H. (2020). Initiation of the Western Pacific Warm Pool at the Middle
1525 Miocene Climate Transition?. *Paleoceanography and Paleoclimatology*, *35*(12),
1526 e2020PA003920. https://doi.org/10.1029/2020PA003920
1527
1528 Spahni, R., Chappellaz, J., Stocker, T. F., Loulergue, L., Hausammann, G., Kawamura, K., ... &
1529 Jouzel, J. (2005). Atmospheric methane and nitrous oxide of the late Pleistocene from Antarctic
1530 ice cores. *Science*, *310*(5752), 1317-1321. DOI: 10.1126/science.abd2897
1531
1532 Spezzaferri, S. (1994). Planktonic foraminiferal biostratigraphy and taxonomy of the Oligocene
1533 and lower Miocene in the oceanic record. An overview. Pacini Editore.
1534
1535 Spezzaferri, S., Kucera, M., Pearson, P. N., Wade, B. S., Rappo, S., Poole, C. R., ... & Stalder, C.
1536 (2015). Fossil and Genetic Evidence for the Polyphyletic Nature of the Planktonic Foraminifera"
1537 Globigerinoides", and Description of the New Genus Trilobatus. *PLoS One*, *10*(5), e0128108.
1538 https://doi.org/10.1371/journal.pone.0128108
1539

Stanley, S. M., & Hardie, L. A. (1998). Secular oscillations in the carbonate mineralogy of reef-building and sediment-producing organisms driven by tectonically forced shifts in seawater chemistry. *Palaeogeography, Palaeoclimatology, Palaeoecology*, *144*(1-2), 3-19. https://doi.org/10.1016/S0031-0182(98)00109-6

Steinke, S., Groeneveld, J., Johnstone, H., & Rendle-Bühring, R. (2010). East Asian summer monsoon weakening after 7.5 Ma: evidence from combined planktonic foraminifera Mg/Ca and δ18O (ODP Site 1146; northern South China Sea). *Palaeogeography, Palaeoclimatology, Palaeoecology*, *289*(1-4), 33-43. https://doi.org/10.1016/j.palaeo.2010.02.007

Steinthorsdottir, M., Coxall, H. K., De Boer, A. M., Huber, M., Barbolini, N., Bradshaw, C. D., ... & Strömberg, C. A. E. (2021). The Miocene: The future of the past. *Paleoceanography and Paleoclimatology*, *36*(4), e2020PA004037. https://doi.org/10.1029/2020PA004037

Stoll, H. M., Guitian, J., Hernandez-Almeida, I., Mejia, L. M., Phelps, S., Polissar, P., ... & Ziveri, P. (2019). Upregulation of phytoplankton carbon concentrating mechanisms during low CO2 glacial periods and implications for the phytoplankton pCO2 proxy. *Quaternary Science Reviews*, *208*, 1-20. https://doi.org/10.1016/j.quascirev.2019.01.012

Stoll, H. M., Schrag, D. P., & Clemens, S. C. (1999). Are seawater Sr/Ca variations preserved in Quaternary foraminifera?. *Geochimica et Cosmochimica Acta*, *63*(21), 3535-3547. https://doi.org/10.1016/S0016-7037(99)00129-5

Stults, D. Z., Wagner-Cremer, F., & Axsmith, B. J. (2011). Atmospheric paleo-CO2 estimates based on Taxodium distichum (Cupressaceae) fossils from the Miocene and Pliocene of Eastern North America. *Palaeogeography, Palaeoclimatology, Palaeoecology*, *309*(3-4), 327-332. https://doi.org/10.1016/j.palaeo.2011.06.017

Super, J. R., Thomas, E., Pagani, M., Huber, M., O'Brien, C. L., & Hull, P. M. (2020). Miocene Evolution of North Atlantic Sea Surface Temperature. *Paleoceanography and Paleoclimatology*, *35*(5), e2019PA003748. https://doi.org/10.1029/2019PA003748

Tanner, T., Hernández-Almeida, I., Drury, A. J., Guitián, J., & Stoll, H. (2020). Decreasing atmospheric CO2 during the late Miocene Cooling. *Paleoceanography and Paleoclimatology*, e2020PA003925. https://doi.org/10.1029/2020PA003925

Tauxe, L., & Feakins, S. J. (2020). A reassessment of the chronostratigraphy of late Miocene C3–C4 transitions. *Paleoceanography and Paleoclimatology*, *35*(7), e2020PA003857. https://doi.org/10.1029/2020PA003857

Thadathil, P., Muraleedharan, P. M., Rao, R. R., Somayajulu, Y. K., Reddy, G. V., & Revichandran, C. (2007). Observed seasonal variability of barrier layer in the Bay of Bengal. *Journal of Geophysical Research: Oceans*, *112*(C2). https://doi.org/10.1029/2006JC003651

Thirumalai, K., Quinn, T. M. & Marino, G. (2016). Constraining past seawater $\delta^{18}O$ and temperature records developed from foraminiferal geochemistry. Paleoceanography 31, 1409-1422. https://doi.org/10.1002/2016PA002970

Thomas, E. K., Clemens, S. C., Sun, Y., Prell, W. L., Huang, Y., Gao, L., ... & Liu, Z. (2016). Heterodynes dominate precipitation isotopes in the East Asian monsoon region, reflecting interaction of multiple climate factors. *Earth and Planetary Science Letters*, *455*, 196-206. https://doi.org/10.1016/j.epsl.2016.09.044

Thomson, D.J., 1982. Spectrum estimation and harmonic analysis. Proceedings of the IEEE 70, 1055- 1096. https://doi.org/10.1109/PROC.1982.12434

Tian, J., Ma, W., Lyle, M. W., & Shackford, J. K. (2014). Synchronous mid-Miocene upper and deep oceanic δ13C changes in the east equatorial Pacific linked to ocean cooling and ice sheet expansion. *Earth and Planetary Science Letters*, *406*, 72-80. https://doi.org/10.1016/j.epsl.2014.09.013

1602 Tierney, J. E., Malevich, S. B., Gray, W., Vetter, L., & Thirumalai, K. (2019). Bayesian
1603 calibration of the Mg/Ca paleothermometer in planktic foraminifera. *Paleoceanography and*
1604 *Paleoclimatology*, *34*(12), 2005-2030. https://doi.org/10.1029/2019PA003744
1605
1606 Tierney, J. E., & Tingley, M. P. (2015). A TEX 86 surface sediment database and extended
1607 Bayesian calibration. *Scientific data*, *2*(1), 1-10. https://doi.org/10.1038/sdata.2015.29
1608
1609 Tierney, J. E., & Tingley, M. P. (2018). BAYSPLINE: A new calibration for the alkenone
1610 paleothermometer. *Paleoceanography and Paleoclimatology*, *33*(3), 281-301.
1611 https://doi.org/10.1002/2017PA003201
1612
1613 Timmermann, R., Goosse, H., Madec, G., Fichefet, T., Ethe, C., & Duliere, V. (2005). On the
1614 representation of high latitude processes in the ORCA-LIM global coupled sea ice–ocean
1615 model. *Ocean Modelling*, *8*(1-2), 175-201. https://doi.org/10.1016/j.ocemod.2003.12.009
1616
1617 Tomczak M, Godfrey JS (2001) Regional Oceanography: an introduction, Chapter 11, The
1618 Indian Ocean, pp 175–198, Chapter 12, hydrology of the Indian Ocean pp199-214.
1619
1620 Unger, D., Ittekkot, V., Schäfer, P., Tiemann, J., & Reschke, S. (2003). Seasonality and
1621 interannual variability of particle fluxes to the deep Bay of Bengal: influence of riverine input
1622 and oceanographic processes. *Deep Sea Research Part II: Topical Studies in*
1623 *Oceanography*, *50*(5), 897-923. https://doi.org/10.1016/S0967-0645(02)00612-4
1624
1625 Valcke, S. (2013). The OASIS3 coupler: A European climate modelling community
1626 software. *Geoscientific Model Development*, *6*(2), 373-388. https://doi.org/10.5194/gmd-6-373-
1627 2013
1628
1629 Van der Weijst, C. M., van der Laan, K. J., Peterse, F., Reichart, G. J., Sangiorgi, F., Schouten,
1630 S., ... & Sluijs, A. (2021). A fifteen-million-year surface-and subsurface-integrated TEX 86
1631 temperature record from the eastern equatorial Atlantic. *Climate of the Past Discussions*, 1-23.
1632 https://doi.org/10.5194/cp-2021-92

Vidya, P. J., Prasanna Kumar, S., Gauns, M., Verenkar, A., Unger, D., & Ramaswamy, V. (2013). Influence of physical and biological processes on the seasonal cycle of biogenic flux in the equatorial Indian Ocean. *Biogeosciences*, *10*(11), 7493-7507. https://doi.org/10.5194/bg-10-7493-2013

Vinayachandran, P. N., & Shetye, S. R. (1991). The warm pool in the Indian Ocean. *Proceedings of the Indian Academy of Sciences-Earth and Planetary Sciences*, *100*(2), 165-175. https://doi.org/10.1007/BF02839431

Visser, K., Thunell, R., & Stott, L. (2003). Magnitude and timing of temperature change in the Indo-Pacific warm pool during deglaciation. *Nature*, *421*(6919), 152-155. https://doi.org/10.1038/nature01297

Wang, C., & Enfield, D. B. (2001). The tropical Western Hemisphere warm pool. *Geophysical research letters*, *28*(8), 1635-1638. https://doi.org/10.1029/2000GL011763

Warnke, D. A., Allen, C. P., Muller, D. W., Hodell, D. A., & Brunner, C. A. (1992). Miocene-Pliocene Antarctic glacial evolution: A synthesis of ice-rafted debris, stable isotope, and planktonic foraminiferal indicators, ODP Leg 114. *The Antarctic Paleoenvironment: A Perspective on Global Change: Part One*, *56*, 311-326. https://doi.org/10.1029/AR056p0311

Webster, P. J., Magana, V. O., Palmer, T. N., Shukla, J., Tomas, R. A., Yanai, M. U., & Yasunari, T. (1998). Monsoons: Processes, predictability, and the prospects for prediction. *Journal of Geophysical Research: Oceans*, *103*(C7), 14451-14510. https://doi.org/10.1029/97JC02719

Westerhold, T., Marwan, N., Drury, A. J., Liebrand, D., Agnini, C., Anagnostou, E., ... & Zachos, J. C. (2020). An astronomically dated record of Earth's climate and its predictability over the last 66 million years. *Science*, *369*(6509), 1383-1387. DOI: 10.1126/science.aba6853

Wilkinson, B. H. & Algeo, T. J. (1989). Sedimentary carbonate record of calcium-magnesium cycling. *American Journal of Science*, *289*, 1158-1194. https://doi.org/10.2475/ajs.289.10.1158

Zachos, J., Pagani, M., Sloan, L., Thomas, E., & Billups, K. (2001). Trends, rhythms, and aberrations in global climate 65 Ma to present. *science*, *292*(5517), 686-693. https://dx.doi.org/10.1126/science.1059412

Zachos, J. C., Quinn, T. M., & Salamy, K. A. (1996). High-resolution (104 years) deep-sea foraminiferal stable isotope records of the Eocene-Oligocene climate transition. *Paleoceanography*, *11*(3), 251-266. https://doi.org/10.1029/96PA00571

Yan, X. H., Ho, C. R., Zheng, Q., & Klemas, V. (1992). Temperature and size variabilities of the Western Pacific Warm Pool. *Science*, *258*(5088), 1643-1645. DOI: 10.1126/science.258.5088.1643

You, Y., & Tomczak, M. (1993). Thermocline circulation and ventilation in the Indian Ocean derived from water mass analysis. *Deep Sea Research Part I: Oceanographic Research Papers*, *40*(1), 13-56. https://doi.org/10.1016/0967-0637(93)90052-5

Zhang, Y. G., Pagani, M., & Liu, Z. (2014). A 12-million-year temperature history of the tropical Pacific Ocean. *Science*, *344*(6179), 84- 87. DOI: 10.1126/science.1246172

Zhang, Y. G., Pagani, M., Liu, Z., Bohaty, S. M., & DeConto, R. (2013). A 40-million-year history of atmospheric CO2. *Philosophical Transactions of the Royal Society A: Mathematical, Physical and Engineering Sciences*, *371*(2001), 20130096. https://doi.org/10.1098/rsta.2013.0096

Zhang, Z., Ramstein, G., Schuster, M., Li, C., Contoux, C., & Yan, Q. (2014). Aridification of the Sahara desert caused by Tethys Sea shrinkage during the Late Miocene. *Nature*, *513*(7518), 401-404. https://doi.org/10.1038/nature13705

1695 Zhu, J., Poulsen, C. J., & Tierney, J. E. (2019). Simulation of Eocene extreme warmth and high
1696 climate sensitivity through cloud feedbacks. *Science advances*, *5*(9), eaax1874. DOI:
1697 10.1126/sciadv.aax1874
1698
1699 Zhuang, G., Pagani, M., & Zhang, Y. G. (2017). Monsoonal upwelling in the western Arabian
1700 Sea since the middle Miocene. *Geology*, *45*(7), 655-658. https://doi.org/10.1130/G39013.1
1701
1702 Zweng, M. M., J. R. Reagan, D. Seidov, T. P. Boyer, R. A. Locarnini, H. E. Garcia, A. V.
1703 Mishonov, O. K. Baranova, K. Weathers, C. R. Paver, and I. Smolyar, 2018. *World Ocean Atlas*
1704 *2018, Volume 2: Salinity*. A. Mishonov Technical Ed.; NOAA Atlas NESDIS 82, 50pp.
1705 http://doi.org/10.7289/V5251G4D